NASA Cross-track Infrared Sounder (CrIS) Level 1B Delta Algorithm Theoretical Basis Document (ATBD)

University of Maryland Baltimore County Atmospheric Spectroscopy Laboratory

University of Wisconsin-Madison Space Science and Engineering Center

Version 3

Product Version: 3
Software Version: 3.0.1

June 2021

This research was conducted with funding provided by the National Aeronautics and Space Administration.

CrIS L1B Science and Software Team

Joe Taylor – PI	UW-Madison
Larrabee Strow – PI	UMBC
Jessica Braun	UW-Madison
Dan Deslover	UW-Madison
Michelle Feltz	UW-Madison
Ray Garcia	UW-Madison
Robert Knuteson	UW-Madison
Graeme Martin	UW-Madison
Howard Motteler	UMBC
Greg Quinn	UW-Madison
Hank Revercomb	UW-Madison
Will Roberts	UW-Madison
Dave Tobin	UW-Madison

Revisions:

Draft	24 Nov 2015	Creation of initial draft document
Version 1.0Beta2	05 Feb 2016	Release consistent with Beta2 software
Version 1.0Beta3	15 Mar 2016	Release consistent with Beta3 software
Version 1.0	01 May 2017	Release consistent with 1.0 software
Version 2.0	10 May 2018	Release consistent with 2.0 software
Version 2.1	24 Jan 2019	Release consistent with 2.1 software, 2.11 product
Version 3	10 Jun 2021	Release consistent with 3.0.1 software, 3 product

Contacts

Readers seeking additional information about this study may contact the following researchers:

CrIS L1B Support Team cris.l1b.support@ssec.wisc.edu

Abstract

This document describes the theoretical basis of the NASA CrIS Level 1B (L1B) algorithm software and resulting product. Because the theoretical basis is very similar to that of the operational Joint Polar Satellite System (JPSS) Sensor Data Record (SDR) algorithm, it was decided to implement this document as a "delta" ATBD describing the differences between the two approaches, rather than implementing a full ATBD with duplicate information. Thus this delta ATBD together with the CrIS SDR ATBD form a complete description of the theoretical basis of the NASA CrIS L1B software.

Table of Contents

Figures

Tables

1 INTRODUCTION

1.1 Purpose of Document

This document describes the theoretical basis of the NASA CrIS Level 1B (L1B) algorithm software and resulting product.

1.2 Scope

The scope of this document is:

- Version 3.0.1 of the NASA CrIS L1B software, and
- Version 3 of the NASA CrIS L1B product

The software was developed by the CrIS L1B Science and Software Team, located at the University of Wisconsin-Madison Space Science and Engineering Center and the University of Maryland Baltimore County Atmospheric Spectroscopy Laboratory.

The product was generated by the SNPP Sounder Science Investigator-led Processing System (SIPS), located at the NASA Jet Propulsion Laboratory (JPL) and Goddard Earth Sciences Data Information Services Center (GES DISC).

1.3 Document Overview

Because the theoretical basis is very similar to that of the operational Joint Polar Satellite System (JPSS) Sensor Data Record (SDR) algorithm, it was decided to implement this document as a "delta" ATBD describing the differences between the two approaches, rather than implementing a full ATBD with duplicate information. Thus this delta ATBD together with the CrIS SDR ATBD form a complete description of the theoretical basis of the NASA CrIS L1B software.

The CrIS SDR ATBD that is a companion to this document was released December 23, 2014 by the JPSS Ground Project, and is called “Joint Polar Satellite System (JPSS) Cross Track Infrared Sounder (CrIS) Sensor Data Records (SDR) Algorithm Theoretical Basis Document (ATBD), Rev C, Code 474, 474-00032”.

The layout of this document corresponds to the layout of the CrIS SDR ATBD. Each section of this document describes the changes relative to the corresponding section in the CrIS SDR ATBD, or the words “No change” indicating there are no changes to be applied.

There are a few cases where the layout of this document does *not* match the layout of the CrIS SDR ATBD, noted here:

- Section 1.6 Notation and Symbols: sub-sections are omitted
- Section 3.3 Fringe Count Error Handling is organized into different sub-sections
- Section 3.4 describes ICT Outlier Handling in addition to Lunar Intrusion, and is organized into different sub-sections
- Section 3.9 Doppler Shift Correction is added
- Section 3.10 Weak Cosine Apodization of Interferograms is added
- Section 7.5.5 Polarization Correction and sub-sections are added

1.4 Reference Documents

The following references are added to the references in the CrIS SDR ATBD.

1. Joint Polar Satellite System (JPSS) Cross Track Infrared Sounder (CrIS) Sensor Data Records (SDR) Algorithm Theoretical Basis Document (ATBD), Rev C, Code 474, 474-00032

2. Joint Polar Satellite System (JPSS) Visible Infrared Imaging Radiometer Suite (VIIRS) Sensor Data Record (SDR) Geolocation Algorithm Theoretical Basis Document (ATBD), E/RA-00004, Rev. A

3. Interface Control Document between Earth Observing System (EOS) Data and Operations System (EDOS) and Science Investigator-led Processing Systems for the Suomi National Polar-Orbiting Partnership (SNPP) Science Data Segment (SDS), 423-ICD-010, Original, Earth Science Data Information Systems (ESDIS), Code 423

4. NASA SNPP Cross Track Infrared Sounder (CrIS) Level 1B Product Users' Guide, Version 3, Rev A

5. Cross-track Infrared Sounder (CrIS) Level 1B Quality Flags Description Document, Version 3

6. CrIS L1B Software Users' Guide, Version 3.0

7. [Montenbruck2000] Montenbruck, O & Gill, Eberhard. (2000). Real-Time Estimation of SGP4 Orbital Elements from GPS Navigation Data.

8. [Han2018] Y. Han and Y. Chen, "Calibration Algorithm for Cross-Track Infrared Sounder Full Spectral Resolution Measurements," in IEEE Transactions on Geoscience and Remote Sensing, vol. 56, no. 2, pp. 1008-1016, Feb. 2018.doi: 10.1109/TGRS.2017.2757940

9. [Revercomb1988] Revercomb, H.E., et al., "Radiometric calibration of IR Fourier transform spectrometers: solution to a problem with the High-Resolution Interferometer Sounder", Applied Optics, 1988. 27(15): p. 3210-3218.

10. [Taylor2014] Taylor, J.K., "Achieving 0.1 K absolute calibration accuracy for high spectral resolution infrared and far infrared climate benchmark measurements", in Génie électrique et génie informatique. 2014, Université Laval.

11. [Taylor2018] Taylor, J. K., Revercomb, H. E., & Tobin, D. C. (2018, November). An analysis and correction of polarization induced calibration errors for the cross-track infrared sounder (CrIS) sensor. In *Fourier Transform Spectroscopy* (pp. FW2B-3). Optical Society of America.

12. [Butler2012] Butler, J.J., Xiong, X., Barnes, R.A., Patt, F.S., Sun, J. and Chiang, K., “An overview of Suomi NPP VIIRS calibration maneuvers”, In Earth Observing Systems XVII (Vol. 8510, p. 85101J). International Society for Optics and Photonics.

1.5 Acronyms

In addition to the acronyms defined in the CrIS SDR ATBD, the following acronyms are used throughout this document.

DM	Diagnostic Mode
EDOS	EOS Data and Operations System
EOS	Earth Observing System
FIFO	First In First Out
FSR	Full Spectral Resolution
GES DISC	Goddard Earth Sciences Data and Information Services Center
J1	NOAA-20 / JPSS-1 Satellite
JPL	Jet Propulsion Laboratory
L1A	Level 1A
L1B	Level 1B
L2	Level 2
LW	Long-wave Infrared
MOPD	Maximum Optical Path Difference
MW	Mid-wave Infrared
NM	Normal Mode
NSR	Normal Spectral Resolution
SIPS	Science Investigator-led Processing System
SNPP	Suomi NPP Satellite
SW	Short-wave Infrared
XSR	Extended Spectral Resolution

1.6 Notations and Symbols

Notational changes have been made to make this document self-consistent. The meanings of the symbols are defined where they are used.

2 SDR ALGORITHMS PRINCIPLES

The primary input to the L1B software is L0 data, which is composed of raw CCSDS packets as received from the spacecraft, together with added metadata. L0 data is produced and distributed by EDOS, and is equivalent to RDR data in the operational JPSS processing system. The L1B software generates L1A and L1B product files. The L1A product contains unpacked spacecraft telemetry data that has been granulated and geolocated, as well as quality flags and metadata. There is no equivalent to the CrIS L1A product in the current operational JPSS processing system. The L1B product contains calibrated spectra, together with geolocation information, quality flags, diagnostic information and metadata. L1B is equivalent to SDRs in the current operational processing system. The L1B product is used as input to L2 processing (equivalent to EDRs in the current operational processing system).

2.1 Objective of the SDR Algorithms

No change.

2.2 Space Segment Signal Processing

No change.

2.2.1 Spikes Detection/Correction

The spike detection and correction of raw interferogram data that is completed by hardware and software on the CrIS sensor is documented in the reference ATBD document. As noted in the reference ATBD document, interferogram spikes are typically associated with impulse noise due to direct bombardment of the CrIS detectors and associated electronics by high energy cosmic particles.

Additional spike detection is implemented in the NASA L1B processing, and Earth scene observations affected by detectable spikes are recorded in the “Earth Scene (ES) Interferogram Spike Detected” quality flag. A spike correction algorithm is not included in the current NASA L1B processing.

The Earth Scene interferogram spike detection is completed after the ICT outlier and DS lunar intrusion detection and removal steps have been completed and the ICT and DS moving averages have been formed on the FOV dependent sensor grid. These are described in Section 3.4. The ICT outlier and DS lunar intrusion detection and removal will identify and discard ICT and DS interferograms with spikes large enough to be detected by those algorithms. The following steps are completed to detect spikes in the Earth scene interferograms.

1. Calculate $R_1 = f_{tukey} \cdot imag\left(\left(\tilde{S}^{es} - \left\langle \tilde{S}^{ds} \right\rangle\right) \Big/ \left(\left\langle \tilde{S}^{it} \right\rangle - \left\langle \tilde{S}^{ds} \right\rangle\right)\right)$, for all Earth scene observations, where f_{tukey} is a tapered cosine window that tapers to zero inside the output range for the band, $\tilde{S}^{es}$ is the complex valued Earth scene spectrum, $\left\langle \tilde{S}^{ds} \right\rangle$ is the complex valued deep

space moving averaged spectrum, and $\langle \tilde{S}^{it} \rangle$ is the complex valued ICT moving averaged spectrum. The function imag() extracts the imaginary part of the complex ratio.

2. For each field of view and field of regard, calculate the mean of R_1 over all scans in the granule and subtract the mean from R_1. This removes any low frequency dependence of R_1.
3. Calculate the Power Spectral Density of R_1 and compare to a sensor and detector dependent threshold. If there are any values of $PSD(R_1)$ that exceed the threshold, then set the "Earth Scene (ES) Interferogram Spike Detected" quality flag for that observation to indicate a spike was detected.

2.2.2 Filtering and Decimation

These additional figures illustrate the actual FIR filter used in the CrIS data processing and the spectral transform of it compared to a typical unfiltered signal.

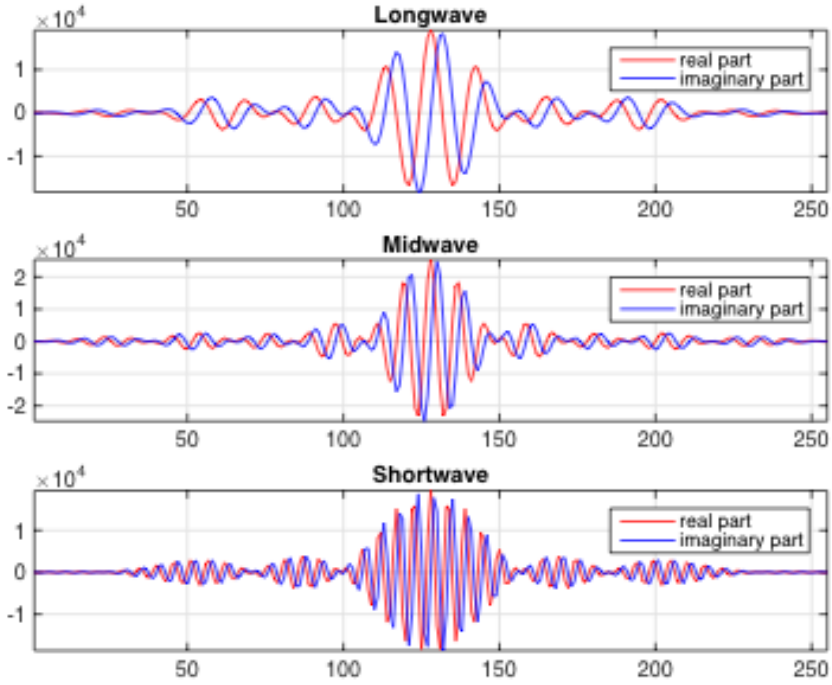

Figure 2.2.2- 1. Complex FIR filters used for the CrIS sensor to suppress out of band signal and noise for each of the longwave, midwave, and shortwave bands.

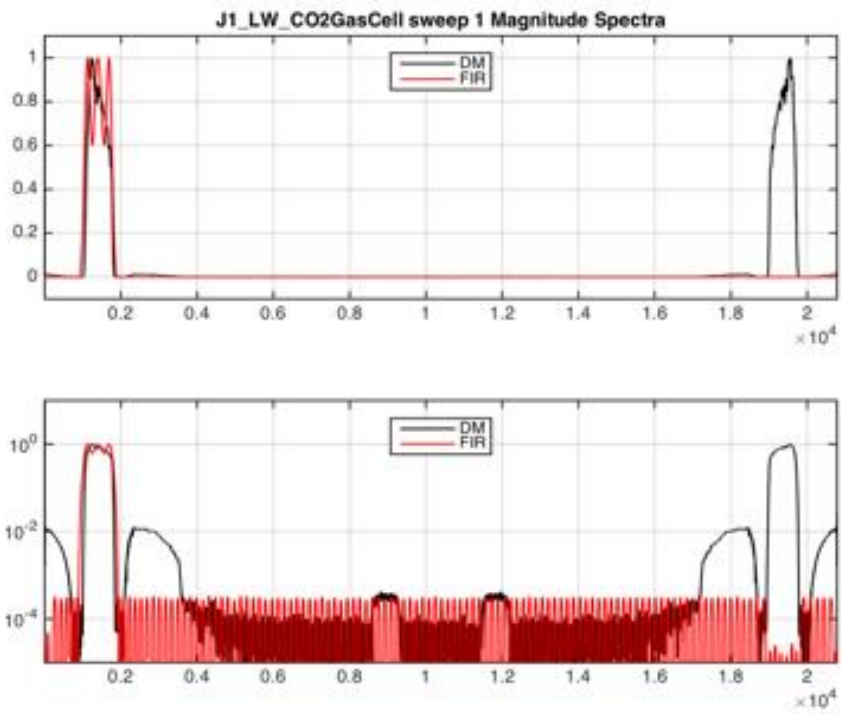

Figure 2.2.2- 2. CrIS longwave band undecimated signal (DM) overlaid with FFT of corresponding FIR filter (FIR). Each curve is normalized to unity.

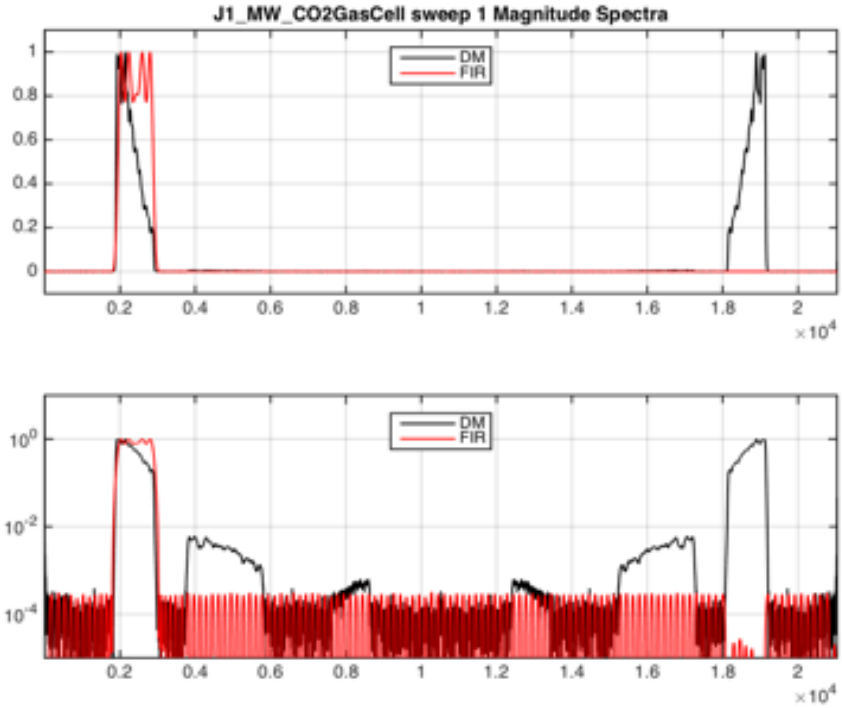

Figure 2.2.2- 3. CrIS midwave band undecimated signal (DM) overlaid with FFT of corresponding FIR filter (FIR). Each curve is normalized to unity.

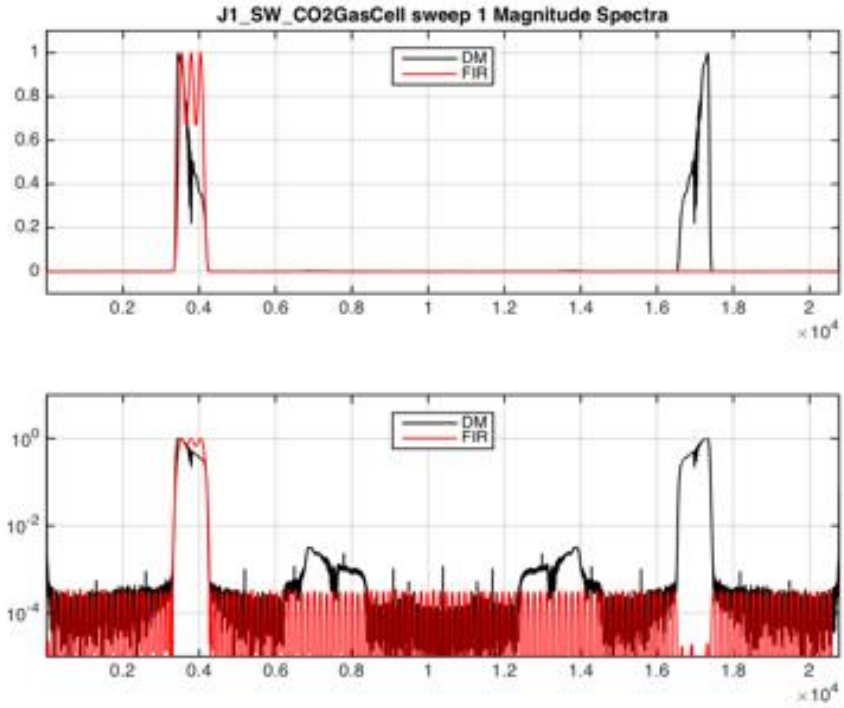

Figure 2.2.2- 4. CrIS shortwave band undecimated signal (DM) overlaid with FFT of corresponding FIR filter (FIR). Each curve is normalized to unity.

2.2.3 Bit Trimming

No change.

2.2.4 Packet Encoding

No change.

2.3 Ground Segment Processing

No change.

2.4 Interferometer Model

No change.

2.4.1 Instrument Phase

No change.

2.4.2 Other Signal Contributors

No change.

2.4.3 Instrument Line Shape

No change.

2.4.4 Other Types of Errors

No change.

2.4.5 Interferometer Modeling Equations

No change.

2.5 CrIS Characteristics

No change.

2.5.1 Double-Sided Interferogram Measurements

No change.

2.5.2 CrIS Spectral Bands

For the first part of the SNPP mission, the effective spectral resolution of CrIS data received from the satellite was lower in the short-wave and mid-wave infrared bands than in the long-wave infrared band. Level 0 data received during this initial period is referred to as Normal Spectral Resolution (NSR). Table 2 and Figure 14 in the SDR ATBD correctly state the spectral sampling of the calibrated radiances for the original low resolution SNPP CrIS data collection mode.

On 4 December 2014 (15:06 UTC), the resolution of the short-wave and mid-wave data transmitted from the SNPP satellite was increased to match the long-wave resolution. Level 0 data received during this period is referred to as Full Spectral Resolution (FSR). After the transition to FSR, the effective spectral resolution of short-wave data received on the ground was quadrupled, and the effective spectral resolution of mid-wave data was doubled, with the Level 0 data volume increasing accordingly.

On 2 November 2015 (16:06 UTC), the SNPP satellite began transmitting long-wave and short-wave interferograms with extra points on the ends. These points had previously been discarded, but were added to the data stream because it was determined that they could be used to improve the quality of the calibration for the FSR radiances. Level 0 data received during this period is referred to as Extended Spectral Resolution (XSR).

The J1 satellite has transmitted CrIS data at XSR for the entire mission to date.

The SNPP L1B product includes datasets at two different spectral resolutions, to meet the goals of providing a spectrally consistent product with the longest possible duration and also with the highest possible spectral resolution. These L1B datasets are referred to as NSR and FSR. The J1 L1B product is produced only at FSR.

For more information on the resolution of the CrIS L1B product datasets, refer to the NASA CrIS L1B Product Users' Guide, Version 3, Rev A.

2.5.3 CrIS Field of Regard

No change.

2.5.4 CrIS Measurement Sequence

No change.

2.5.5 CrIS Signal Processing

The SDR ATBD Table 4 represents the interferogram number of points at launch of SNPP during the NSR data collection period. The following table summarizes the interferogram data processed using the NASA CrIS L1B software as described in Section 2.5.2 of this document. The label DM (Diagnostic Mode) indicates the number of interferogram points prior to the on-orbit application of the FIR filter (see Section 2.2.2). The label NM (Normal Mode) indicates the number of interferogram points output by the FIR filter and downlinked from the satellite to the ground.

Table 2.5.5- 1. Number of interferogram points before and after on-board filtering.

CrIS Data Mode	LW	MW	SW
NM SNPP NSR	866	530	202
NM SNPP FSR	866	1052	799
NM SNPP XSR	874	1052	808
NM JPSS1 XSR	876	1052	808
Decimation Factor	24	20	26
DM SNPP NSR	866*24+254	530*20+254	202*26+254
DM SNPP FSR	866*24+254	1052*20+254	799*26+254
DM SNPP XSR	874*24+254	1052*20+254	808*26+254

DM JPSS1 XSR	876*24+254	1052*20+254	808*26+254

2.6 Signal Representation

No change.

2.6.1 Array Dimensions

No change.

2.6.2 Data Ordering

No change.

3 SPECIAL CONSIDERATIONS

3.1 Non-linearity Correction

No change.

3.2 Scan Mirror Polarization Compensation

The CrIS sensor utilizes a “barrel-roll” scene select mirror that rotates about an axis that is 45° from the mirror normal, preserving the angle of incidence at the mirror for all calibration and scene views. It is well known that the reflection from an inclined metallic surface will always induce some polarization. An uncoated gold scene select mirror was chosen for CrIS due to its extremely low polarization in the infrared. As a first order effect, the magnitude of polarization induced by the 45° scene select mirror will be constant for all scene select mirror rotation angles, since the incident angle at the scene mirror is constant regardless of rotation angle. Secondly, the polarization induced by the other components in the instrument CrIS optical chain, including the interferometer and aft-optics, is not dependent on the position of the 45° scene mirror, and is constant for all scene mirror positions.

However, the plane of reflection at the scene mirror rotates with the scene mirror rotation and thus the polarization plane angle of the scene select mirror partial polarization will depend on the scene select mirror rotation angle. The polarization sensitivity and polarization plane of the rest of the sensor optical chain is constant and independent of the scene mirror rotation angle. It is expected that the sensor polarization (not including the scene mirror) is primarily due to the beamsplitter and aft-optic dichroics but also includes contributions from the other optical elements within the sensor. As a result, it can be understood that the rotation of the reflection plane at the scene mirror will create a modulation of the signal measured at the detector. Early analysis, which only included transmission effects, prior to the launch of SNPP CrIS indicated that this was not expected to be a significant effect for the CrIS sensor. However, when the polarized emission from the scene mirror is included in the analysis, the effect becomes non-negligible for cold scenes and a correction is warranted.

When considering the calibration bias due to polarization, representing the scene select mirror and sensor as a series pair of partial linear polarizers helps provide insight into the problem. The first polarizer represents the polarization due to the scene select mirror and the second polarizer represents the sensor polarization sensitivity. While the level of polarization is constant for the scene select mirror and sensor individually, the combined polarization due to the scene select mirror and the sensor is a function of the relative angle between the scene select mirror polarization axis which changes with rotation of the scene select mirror, and the instrument polarization axis, which is fixed and oriented at a constant angle α. Thus, the combined polarization depends on the scene mirror rotation angle, and the rotation of the reflection plane at the scene mirror will create a modulation of the measured signal.

A relationship between the correct calibrated radiance $L_s(\sigma)$ and the calibrated radiance affected by the calibration bias due to polarization $L_{\delta S}(\sigma)$ can be defined:

$$L_S(\sigma) = L_{\delta,S}(\sigma) - E_p(\delta,\sigma) \qquad [3.2.1]$$

where σ denotes the wavenumber scale, and $E_p(\delta_S,\sigma)$ is the polarization induced calibration bias at scene select mirror angle δ_S . The radiometric calibration of the CrIS sensor uses the complex calibration method described by Revercomb [Revercomb1988], and it can be shown [Taylor2014, Taylor2018] that the calibration bias due to polarization for the CrIS instrument at a given scene mirror angle δ_S and instrument polarization axis angle σ is accurately represented as

$$E_p(\delta,\sigma) \cong p_r p_t \left\{ \begin{array}{l} L_S \cos 2(\delta_S - \alpha) - L_{ICT} \dfrac{L_S - L_{DS}}{L_{ICT} - L_{DS}} \cos 2(\delta_{ICT} - \alpha) - L_{DS} \dfrac{L_{ICT} - L_S}{L_{ICT} - L_{DS}} \cos 2(\delta_{DS} - \alpha) \\ -B_{SSM} \left[\cos 2(\delta_S - \alpha) - \dfrac{L_S - L_{DS}}{L_{ICT} - L_{DS}} \cos 2(\delta_{ICT} - \alpha) - \dfrac{L_{ICT} - L_S}{L_{ICT} - L_{DS}} \cos 2(\delta_{DS} - \alpha) \right] \end{array} \right\}$$

[3.2.2]

where p_r is the polarization of the scene select mirror, p_t is the sensor polarization, L_{ICT} and L_{DS} are the predicted radiances for the respective ICT and deep space calibration views, δ_S is the scene mirror angle of the observation, δ_{ICT} and δ_{DS} are the scene mirror angles for the respective ICT and deep space calibration views, and B_{SSM} is radiance from a blackbody at the temperature of the scene selection mirror. $p_r, p_t, L_{ICT}, L_{DS}, L_S$ are spectrally resolved parameters, while a single value for each detector band is used for α.

The polarization correction, as described by Equations 3.2.1 and 3.2.2, is applied to the calibrated radiances on the user grid spectral sampling as the last step of the processing chain. For the correction, $L_s(\sigma)$ in equation 3.2.2 is approximated by $L_{\delta,S}(\sigma)$. This is an acceptable approximation when calculating the correction and the associated error is insignificant with respect to the uncertainty in the correction.

A satellite pitch maneuver was conducted for both SNPP [Butler2012] and NOAA-20. The polarization parameters required for the correction were determined using data acquired by the CrIS instrument during the pitch maneuver. During the pitch maneuver, all of the CrIS cross-track fields of regard that normally view the Earth view deep space. In this configuration, field of regard and detector dependent differences are dominated by the instrument polarization, making this an ideal dataset for derivation of the polarization parameters. The raw and calibrated signals show clear polarization effects, and are very well represented by the theoretical model. The parameters for each CrIS sensor spectral band and field of view are represented configuration files of the L1B software.

3.3 Fringe Count Error Handling

A fringe counting system, using a reference laser source within the interferometer subsystem, determines the optical path difference sampling. If, for any reason, a fringe is lost, then the current and the following interferograms are shifted with respect to previous ones. A shift in the time (OPD) domain corresponds to a phase rotation in the frequency (wavenumber) domain. This means that the spectral phase of subsequent measurements will be affected, and if they are calibrated using calibration reference measurements taken before the occurrence of the fringe loss, then errors will be introduced into the final spectrum. The method for detecting and correcting fringe losses is based on the analysis of the residual phase of spectra.

3.3.1 Fringe Count Errors

Fringe count errors (FCEs) can occur anytime during the interferogram acquisition or during the moving mirror turnaround. If they occur during the moving mirror turnaround between successive interferograms the effect is to shift all interferograms following the error. If this remains uncorrected, a phase error will arise because all the measurements involved in the calibration will not have the same optical path difference sampling. A stable instrument is not expected to suffer from this type of error.

If a cosmic ray falls on the metrology system (detector, electronics, etc.), the metrology system could lose one or more fringes during the interferogram acquisition. This type of error can occur anywhere in the interferogram. The effect of “in-sweep” fringe errors is twofold: first it shifts the last part of the interferogram in which the error occurs with respect to the first part. This effect results in a distortion of the current measurement that is very difficult to recover. The second effect is that all subsequent measurements will be shifted with respect to any previous measurements. This latter effect is the same as if the error would have occurred during the turnaround between successive interferograms.

As of the CrIS NASA L1B Version 3.0 software release, only one real case of a fringe count error for SNPP CrIS has occurred over its entire lifetime, and no real FCE’s have been identified for the NOAA-20 / JPSS-1 CrIS instrument.

3.3.2 CrIS ZPD Synchronization

Each time the instrument is powered on or initialized, the interferogram sampling window position is re-established. This is done using a LED interrupter circuit mounted on the interferometer porch swing assembly. This ZPD position is initially used to mark the sampling window position. Following this “coarse” ZPD position determination, the CrIS sensor refines the ZPD centering of the sweep by detecting the maximum absolute value of interferogram sample while viewing the ICT target in the MW band.

This process ensures that ZPD centering is always maintained to within ±12 laser fringe counts of the true ZPD by the CrIS instrument. This shift of the OPD sampling window is not critical since extra samples are collected to assure that the full maximum path difference of the interferometer is achieved for both ends of the sweep.

3.3.3 Phase Analysis

The fringe count error handling consists of two distinct steps: (1) detection and (2) correction. The detection step is optimized to identify potential FCEs while having a minimal impact on processing time. The correction step is only initiated if a potential fringe count error is identified in the detection step, and accordingly can be more resource intensive without impacting the processing time unless an FCE has occurred. The first step of the correction step is the verification of the FCE detection. Since a true fringe count error will affect all 3 detector bands, the detection is only performed for the LW band.

3.3.4 FCE Detection

The approach used for fringe count error (FCE) detection consists of an analysis of the linear wavenumber- dependent residual phase that comes from comparing signals to each other (ES, ICT and DS). When the OPD axis definition of the current Earth scene interferogram is the same as the ICT and DS interferograms used as calibration references, then the residual phase should be zero. A shift in any of them with respect to the others produces a phase error increasing linearly with wavenumber.

Possible fringe count errors are identified by evaluating (1) the phase difference between the Earth and deep space difference (the numerator of the complex calibration equation) and the ICT and deep space difference (the denominator of the complex calibration equation), and (2) the phase difference between the ICT spectra and a reference ICT spectrum. Phase depends on interferometer sweep direction, so forward and reverse sweep observations are tested separately.

$$\Phi_1 = phase\left(\underline{\tilde{S}}^{es} - \underline{\tilde{S}}^{ds}\right) - phase\left(\underline{\tilde{S}}^{it} - \underline{\tilde{S}}^{ds}\right)$$

$$\Phi_2 = phase\left(\underline{\tilde{S}}^{it}\right) - phase\left(\underline{\tilde{S}}^{it}_{ref}\right)$$

The phase differences Φ_1 and Φ_2 are compared to a threshold that corresponds to the phase difference due to approximately half of a single fringe shift, and an observation is flagged as having a possible FCE if either phase difference exceeds the threshold. Since a fringe count error will impact all detector bands, the detection step is only completed on the LW band using the mean phase in the LW window region. The reference ICT spectrum is selected such that it has a phase closest to the phase of the mean ICT spectrum for the ICT spectra ensemble. There are 135 spectra in the ensemble for nominal processing which includes posterior and anterior context granules. FCE detection is conducted independently for each field of view.

3.3.5 FCE Correction

If a fringe count error is detected in all longwave fields of view during a single interferogram acquisition, then the fringe count error correction routine is executed. In the L1B FCE correction, the ICT spectra are used to determine the size of each FCE. Using the ICT spectra is much more robust than using the ES spectra since the spectral features and large range of scene variations in the ES views can complicate phase comparisons due to scene dependent 2π phase wrapping. As described in Section 2.5.4 and illustrated in Figure 3.3.5-1, the typical CrIS cross-track scan measurement sequence consists of 34 interferometer sweeps that include 30 Earth scenes, 2

deep space, and 2 ICT measurements. Accordingly, since the L1B FCE correction uses ICT spectra to determine the size of the fringe count error, the FCE correction will not identify or correct the unlikely case where the accumulated fringe count error in one cross-track scan sequence is zero, but multiple offsetting fringe count errors have occurred in fields of regard 0 through 31 for that scan line.

The fringe count error correction routine is described below. For the same reasons noted in the FCE detection description, the LW window region is used to determine the size of each fringe count error. The following calculations are completed for all fields of view, and independently for each interferometer sweep direction.

1. Calculate Φ_2, the phase difference between each ICT spectrum and the reference ICT spectrum.
2. Calculate the mean phase $\Phi_{\Delta x/DF}$ for the longwave window region (longwave band channels $n_{window} = \left[n_1, n_1 + 1, ..., n_x\right]$) corresponding to a shift of a single undecimated optical path difference sample interval $dx = \Delta x / DF_b$

$$\Phi_{\Delta x/DF_b} = \left\langle 2\pi\sigma\left[n\right]\frac{\Delta x}{DF_b}\right\rangle_{n_{window}}$$

3. Calculate the integer fringe count error k_d^{fce} detected for each ICT spectra. Since there are two ICT observations per scan line, corresponding to forward (0) and reverse (1) interferometer sweep directions, there will be a forward and a reverse k_d^{fce} value for scan-line. If no FCE was detected for that ICT observation, $k_d^{fce} = 0$.

$$k_d^{fce} = round\left(\frac{\Phi_2}{\Phi_{\Delta x/DF_b}}\right)$$

4. Since fringe count errors should be quantized, assume any k_d^{fce} that are not within 0.1 of an integer value prior to rounding are erroneous and set those k_d^{fce} to zero.
5. Calculate the phase rotation for all non-zero integer fringe count error values, and apply that phase rotation to all same sweep direction observations in that scan line.

$$k_d^{fce}\left(j\right)$$

6. Re-run the FCE detection routine to find any Earth scene observations that have phase errors after correction and remove the phase correction for those observations. This addresses two cases: (1) a real FCE occurred during the Earth scene observations for the given scan line, but only the observations acquired after the FCE need correction; (2) the FCE correction has failed for either a real or false FCE detection.

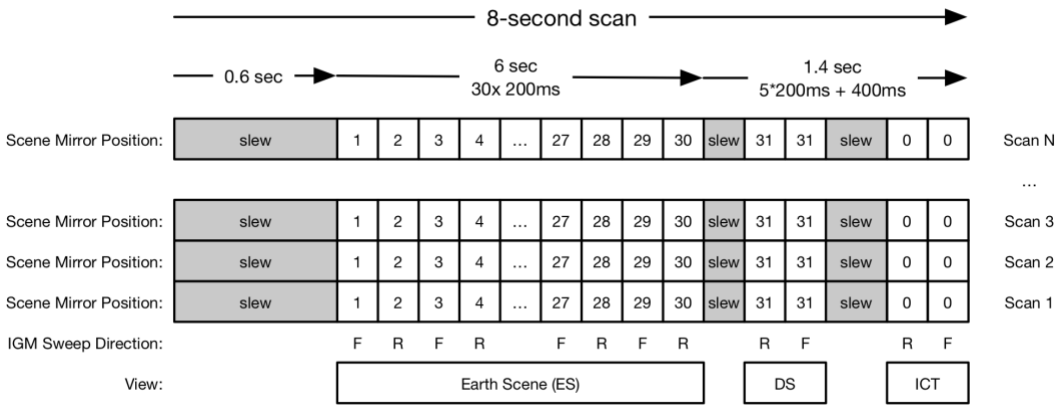

Figure 3.3.5- 1 Multiple cross-track scan lines in the CrIS 8-second measurement sequence. F and R denote sweep direction for interferometer (F = forward sweep direction, R = reverse sweep direction).

FCE detection and failure of FCE correction are recorded in separate quality flags. The FCE detected flag is set for any observations that were identified as having fringe count errors in the fringe count error detection step and verified by the fringe count error correction step. The FCE correction failed flag is set for any observations for which a fringe count error was detected and verified, but could not be resolved by the correction step.

3.4 Lunar Intrusion and ICT Outlier Handling

It is possible that a regular space look data collection will occasionally coincide with a full or partial view of the moon. The space reference spectra that are identified as outliers are flagged as invalid and excluded from the DS moving window average. The detection is done separately for each FOV and for each sweep direction in all 3 bands. Since a lunar view will not fill the full field of regard, it is possible for some FOVs to experience lunar intrusion while others do not. The lunar intrusion detection will also detect deep space view data which are outliers but are not associated with lunar intrusion events.

It is also possible that a regular ICT data collect may be corrupted. While this is extremely rare, a similar outlier detection is also completed separately for each FOV and for each sweep direction in all 3 bands for the ICT data. The ICT spectra that are identified as outliers are flagged as invalid and excluded from the ICT moving window average.

3.4.1 ICT Outlier Detection

ICT outlier detection is completed by comparing the uncalibrated complex valued spectra for all ICT views versus a reference mean ICT spectrum that is ideally free of defects. This is completed independently for all 27 CrIS detectors (9 FOVs in 3 detector bands) and interferometer sweep direction. ICT outlier detection is completed prior to lunar intrusion detection.

The following steps are taken to detect an ICT outlier. ICT spectra from the current and context granules are included in the detection process if context granules have been provided to the processing. The use of context granules provides a larger ensemble of ICT views and more

robust outlier detection. The detection algorithm and thresholds have been optimized for the recommended processing implementation which includes anterior and posterior context granules.

1. Form a mean ICT reference spectrum via iterative z-score outlier detection and exclusion of outliers from the ensemble of ICT spectra. Complete **three** iterations of the following steps a - d:
    a. Calculate the mean uncalibrated (complex) ICT spectrum (band "b", FOV "p", and sweep direction "d" independence), averaged over all scans "k" with outliers removed (no outliers are flagged for first iteration), $\left\langle \tilde{\underline{S}}^{ict}_{b,p,d}[n] \right\rangle_k$
    b. Apply a 100 cm^{-1} wide boxcar smoothing filter to the mean uncalibrated (real and imaginary) ICT spectrum.
    c. Calculate the z-score z^{ict} for all ICT spectra with respect to their respective smoothed mean ICT reference spectrum (with independent calculations for band "b", FOV "p", and sweep direction "d"). The z-score for an individual ICT observation $\tilde{\underline{S}}^{ict}_{b,p,d}[n]$ is calculated as the difference between the observation and the reference mean, divided by the standard deviation σ^{ict}_z of the ensemble of ICT observations (with outliers detected in the previous iteration(s) omitted from the current ensemble). A 100 cm^{-1} wide boxcar smoothing filter is applied to σ^{ict}_z. A separate z-score is calculated for the imaginary and real components of the complex spectra, for every spectral channel within the spectral range defined by the wavenumber limits provided in Table 3.4-1.

$$z^{ict}_{b,p,d}[n] = \frac{\tilde{\underline{S}}^{ict}_{b,p,d}[n] - smooth\left[\left\langle \tilde{\underline{S}}^{ict}_{b,p,d}[n] \right\rangle_k\right]}{smooth\left[\sigma^{ict}_z\right]} \qquad [3.4.1]$$

    d. Index all observations with a z-score magnitude greater than 5 in any spectral channel n within the specified wavenumber range for the real or imaginary component. ICT views corresponding to these indices are considered outliers and are removed from subsequent mean ICT reference calculations within the outlier detection algorithm (including any following iterations of Step 1).
2. Calculate the mean ICT uncalibrated (complex) reference spectrum $\left\langle \tilde{\underline{S}}^{ict}_{b,p,d}[n] \right\rangle_k$ over all scans with outliers identified in Step 1 removed (in band "b", FOV "p", and sweep direction "d").
3. Apply a 100 cm^{-1} wide boxcar smoothing filter to the mean ICT uncalibrated (complex) reference spectrum.
4. Calculate the relative spectral difference between the individual ICT uncalibrated spectra and the spectrally smoothed mean ICT reference spectrum from (in band "b", FOV "p", and sweep direction "d").

$$\tilde{\underline{R}}^{ict}_{b,p,d}[n] = \frac{\tilde{\underline{S}}^{ict}_{b,p,d}[n] - smooth\left[\left\langle \tilde{\underline{S}}^{ict}_{b,p,d}[n] \right\rangle_k\right]}{smooth\left[\left\langle \tilde{\underline{S}}^{ict}_{b,p,d}[n] \right\rangle_k\right]} \qquad [3.4.2]$$

5. Index all observations with a real or imaginary component of the relative spectral difference $\tilde{\underline{R}}^{ict}_{b,p,d}[n]$ that exceed the thresholds defined in Table 3.4-2. The test is completed for all spectral channels within the spectral range defined by the wavenumber limits provided in

Table 3.4-1. ICT observations corresponding to these indices are considered outliers and the ICT outlier flag $IO_{b,p,d,k}$ (band "b", FOV "p", sweep direction "d", scan line "k") is set to 1 (outlier detected) for these ICT observations and they are excluded from the ICT moving window average.

$$IO_{b,p,d,k} = \begin{cases} 0, & \tilde{\underline{R}}^{ict}_{b,p,d}[n] \le \dfrac{IO_{threshold}}{100} \\ 1, & \tilde{\underline{R}}^{ict}_{b,p,d}[n] > \dfrac{IO_{threshold}}{100} \end{cases} \qquad [3.4.3]$$

Table 3.4.1- 1. Lower and upper wavenumber limits for spectral regions used in the ICT outlier detection algorithm.

Detector Band	Lower Limit [cm^{-1}]	Upper Limit [cm^{-1}]
LW	750	900
MW	1310	1500
SW	2255	2425

Table 3.4.1- 2. Threshold values used for ICT outlier detection.

Detector Band	ICT Outlier Threshold (real) [%]		ICT Outlier Threshold (imag) [%]	
	SNPP	J1	SNPP	J1
LW	1	1	2	2
MW	1.5	1	2.5	2.5
SW	2	2	4	4

3.4.2 ICT Outlier Processing

If equation [3.4.3] is true for any specific band "b", FOV "p", sweep direction "d" and cross-track scan sequence line "k", then the ICT spectrum is marked as invalid only for that band, FOV, sweep direction, and scan line. Any ICT measurements marked invalid from this process are excluded from the Moving Window average. For each ICT outlier detection in band "b", FOV "p", sweep direction "d" and cross-track scan sequence line "k", the ICT outlier flag is set in the user-facing quality information for the corresponding Earth observations with the same band, FOV, sweep direction, and line.

3.4.3 Lunar Intrusion Detection

"*On rare instances, the space look measurement used to calibrate the CrIS sensor background may encounter a view of the moon. Typically, this may only occur on one or two FOVs simultaneously and possibly on 2 to 3 successive space looks as the spacecraft orbit progresses past the view of the moon. When this happens, then it is necessary to detect this condition and*

exclude use of this contaminated space look data in the CrIS calibration." [JPSS ATBD CrIS SDR, REV C].

Lunar intrusion detection is completed by comparing the uncalibrated complex valued spectra for all Deep Space views versus a reference mean Deep Space spectrum that is ideally free of defects. This is completed independently for all 27 CrIS detectors (9 FOVs in 3 detector bands) and each interferometer sweep direction.

The following steps are taken to detect a lunar intrusion. Deep space spectra from the current and context granules are included in the detection process if context granules have been provided to the processing. The use of context granules provides a larger ensemble of spectra and more robust outlier detection. The detection algorithm and thresholds have been optimized for the recommended processing implementation which includes anterior and posterior context granules.

1. Form a mean DS reference spectrum via iterative z-score outlier detection and exclusion of outliers from the ensemble of DS spectra. Complete **five** iterations of the following steps a - d:
    a. Calculate the mean uncalibrated (complex) DS spectrum (band "b", FOV "p", and sweep direction "d" independence), averaged over all scans "k" with outliers removed (no outliers are flagged for first iteration), $\left\langle \tilde{\underline{S}}^{ds}_{b,p,d}[n] \right\rangle_k$
    b. Apply a 100 cm^{-1} wide boxcar smoothing filter to the mean uncalibrated (real and imaginary) DS spectrum.
    c. Calculate the z-score z^{ds} for all DS spectra with respect to their respective smoothed mean DS reference spectrum (with independent calculations for band "b", FOV "p", and sweep direction "d"). The z-score for an individual DS observation $\tilde{\underline{S}}^{ds}_{b,p,d}[n]$ is calculated as the difference between the observation and the reference mean, divided by the standard deviation σ^{ds}_z of the ensemble of DS observations (with outliers detected in the previous iteration(s) omitted from the ensemble). A 100 cm^{-1} wide boxcar smoothing filter is also applied to σ^{ds}_z. A separate z-score is calculated for the imaginary and real components of the complex spectra, for every spectral channel within the spectral range defined by the wavenumber limits provided in Table 3.4-3.

$$z^{ds}_{b,p,d} = \frac{\tilde{\underline{S}}^{ds}_{b,p,d}[n] - smooth\left[\left\langle \tilde{\underline{S}}^{ds}_{b,p,d}[n] \right\rangle_k\right]}{smooth\left[\sigma_z\right]} \qquad [3.4.4]$$

    d. Index all observations with a z-score magnitude greater than 4 in any spectral channel n within the specified wavenumber range for the real or imaginary component. DS views corresponding to these indices are considered outliers and are removed from subsequent mean DS reference calculations within the lunar intrusion detection algorithm (including any following iterations of Step 1).
2. Calculate the mean DS uncalibrated (complex) reference spectrum $\left\langle \tilde{\underline{S}}^{ds}_{b,p,d}[n] \right\rangle_k$ over all scans with outliers identified in Step 1 removed (in band "b", FOV "p", and sweep direction "d").
3. Apply a 100 cm-1 wide boxcar smoothing filter to the mean ICT uncalibrated (complex) reference spectrum.

4. Calculate the relative spectral difference between the individual DS uncalibrated spectra and the spectrally smoothed mean DS reference spectrum from (in band “b”, FOV “p”, and sweep direction “d”).

$$\underline{\tilde{R}}^{ds}_{b,p,d}[n] = \frac{\underline{\tilde{S}}^{ds}_{b,p,d}[n] - smooth\left[\left\langle \underline{\tilde{S}}^{ds}_{b,p,d}[n]\right\rangle_k\right]}{smooth\left[\left\langle \underline{\tilde{S}}^{ds}_{b,p,d}[n]\right\rangle_k\right]} \qquad [3.4.5]$$

5. Index all observations with a real or imaginary component of the relative spectral difference $\underline{\tilde{R}}^{ds}_{b,p,d}[n]$ that exceed the thresholds defined in Table 3.4-4. The test is completed for all spectral channels within the spectral range defined by the wavenumber limits provided in Table 3.4-3. DS observations corresponding to these indices are considered to be impacted by lunar intrusion and the lunar intrusion detected flag $LI_{b,p,d,k}$ (band “b”, FOV “p”, sweep direction “d”, scan line “k”) is set to 1 (lunar intrusion detected) for these DS observations and they are excluded from the DS moving window average.

$$LI_{b,p,d,k} = \begin{cases} 0, & \underline{\tilde{R}}^{ds}_{b,p,d}[n] \le \dfrac{LI_{threshold}}{100} \\ 1, & \underline{\tilde{R}}^{ds}_{b,p,d}[n] > \dfrac{LI_{threshold}}{100} \end{cases} \qquad [3.4.6]$$

Table 3.4.3- 1. Lower and upper wavenumber limits for spectral region used in the lunar intrusion detection algorithm.

Detector Band	Lower Limit [cm^{-1}]	Upper Limit [cm^{-1}]
LW	750	900
MW	1310	1500
SW	2255	2425

Table 3.4.3- 2. Threshold values used for lunar detection.

Detector Band	Lunar Intrusion Threshold (real) [%]		Lunar Intrusion Threshold (imag) [%]	
	SNPP	J1	SNPP	J1
LW	0.5	0.5	2.5	2.5
MW	1	1	3.5	3.5
SW	1.5	2.5	5	5

3.4.4 Lunar Intrusion Processing

If equation [3.4.6] is true for any specific band “b”, FOV “p”, sweep direction “d” and cross-track scan sequence line “k”, then the Deep Space spectrum is marked as invalid only for that band,

FOV, sweep direction, and scan line. Any deep space measurements marked invalid from this process are excluded from the Moving Window average. For each lunar intrusion detection in band “b”, FOV “p”, sweep direction “d” and cross-track scan sequence line “k”, the lunar intrusion flag in the user-facing quality information is set for the corresponding Earth observations with the same band, FOV, sweep direction, and line.

3.5 Alignment of Data to a Common Spectral Grid

The primary change for the NASA L1B processing, with respect to CrIS SDR ATBD Section 3.5, is that spectral resampling is performed on the *undecimated* spectral domain.

The F-matrix operator is defined as:

$$F[k,k'] = \frac{\Delta\sigma_s}{\Delta\sigma_u} \frac{\mathrm{Sin}(\pi \frac{\sigma_{s,k'} - \sigma_{u,k}}{\Delta\sigma_u})}{N_O \mathrm{Sin}(\pi \frac{\sigma_{s,k'} - \sigma_{u,k}}{N_O \Delta\sigma_u})} \qquad [3.5.1]$$

where,

$\Delta\sigma_s$ is the sensor spectral grid spacing,

$\Delta\sigma_u$ is the user spectral grid spacing,

$\sigma_{s,k'}$ is the wavenumber for the bin k' on the sensor grid σ_s,

$\sigma_{u,k}$ is the wavenumber for the bin k on the user spectral grid σ_u , and

N_O is the undecimated number of interferogram samples truncated to NSR MOPD (N_O = 20736 for the LW, N_O = 10560 for the MW, and N_O = 5200 for the SW).

The band dependence of the F-operator, $\Delta\sigma_s$, and $\Delta\sigma_u$ is not explicitly noted in equation [3.5.1]. The F-matrix operator is computed separately for each granule using Neon data contained in the most coincident engineering packet.

Wavenumbers assigned to each spectral bin prior to resampling are based on the laser metrology sampling wavelength (see Section 4.1 of the ATBD). The laser λ_L^b value in band “b” is computed by the spectral calibration module and used to recompute the F-matrix operator (based on the calibration neon count). The laser wavelength is stabilized on the CrIS instrument (λ_L^b stable to within +/-0.4 ppm over one orbit).

3.6 ILS Correction

No change.

3.6.1 Introduction

No change.

3.6.2 CrIS Off-Axis Self Apodization

No change.

3.6.3 Self-Apodization Removal

Numerical evaluation of the integral

The Self-Apodization (SA) matrix is calculated as:

$$SA[k',k] = \int_{\sigma_{\min}}^{\sigma_{\max}} d\sigma' \,\mathrm{Psinc}\left(\frac{\sigma_{k'} - \sigma'}{\Delta\sigma_s}, N_O\right) \cdot ILS(\sigma', \sigma_k) \qquad [3.6.1]$$

where,

$$\mathrm{Psinc}(x, N_O) = \frac{\sin(\pi x)}{N_O \sin\left(\pi x / N_O\right)} \qquad [3.6.2]$$

$\Delta\sigma_s$ is the sensor spectral grid spacing

σ_k is the wavenumber for the bin k,

N_O is the undecimated number of interferogram samples truncated to L0 NSR MOPD for the L1B NSR product (N_O = 20784 for the LW, N_O = 10600 for the MW, and N_O = 5252 for the SW), or at the L0 XSR MOPD for the FSR L1B product (N_O = 20976 for the LW, N_O = 21040 for the MW, and N_O = 21008 for the SW)

$ILS(\sigma', \sigma_k)$ is the self apodized instrument line shape distortion due to off axis geometry.

Equation [3.6.1] replaces Equation [41] of the CrIS SDR ATBD (Rev C).

The numerical calculation of the SA matrix described by Equations [3.6.1] and [3.6.2] can create spectral ringing artifacts at the band edges when the wavenumber scale indices k and k' match the number of number of output channels after inversion. To mitigate this effect, a temporary expanded square self-apodization (SA) matrix is used, denoted by SA*. The size of SA* is the number of interferogram points multiplied by an expansion factor, with the center of the SA and SA* wavenumber scales aligned. An expansion factor of 3.0 is used for all 3 bands (LW, MW, and SW) when generating the inverse self-apodization matrix. The inverse of the expanded SA* matrix is calculated, and SA^{-1} is extracted from SA^{*-1}. The use of an expansion factor is described in [Han2018], in Section IV of "Calibration Algorithm for Cross-Track Infrared Sounder Full Spectral Resolution Measurements" (DOI: 10.1109/TGRS.2017.2757940).

The inverse self apodization matrix is calculated offline for each band “b” using a nominal laser metrology sampling wavelength value, $\lambda_{L,ISA}^{b}$. The current laser metrology sampling wavelength for band “b” (λ_{L}^{b}) is determined from the spectral calibration module (based on the neon count). If λ_{L}^{b} differs from $\lambda_{L,ISA}^{b}$ by more than a pre-defined threshold, the ISA degraded QF is set to 1.

3.6.4 Residual Term

The residual term is not calculated.

3.6.5 Guard Band Damping

The calibration filter formulation is the same as that described in the CrIS SDR ATBD document:

$$f_b[k] = \left[\frac{1}{e^{a_2(k_0-a_1-k)}+1}\right]\cdot\left[\frac{1}{e^{a_4(k-k_1-a_3)}+1}\right] \qquad [3.6.3]$$

The parameters for the filter have been optimized for use within the NASA L1B complex calibration procedure. The parameters are provided in Table 3.6.5-1.

To be independent of wave number, equation [3.6.3] is expressed in bins. It is important to note that the bin number range begins at 1, and not at zero. In case the range starts at 0, the three k 's in Table 3.6.5-1 need to be reduced by 1.

Table 3.6.5- 1. Parameters for the calibration filter. NSR and FSR denote L1B product output resolution.

	LW	MW	SW
k	1 - 866 (NSR) 1 - 874 (SNPP FSR) 1 - 876 (J1 FSR)	1 – 530 (NSR) 1 - 1052 (FSR)	1 – 202 (NSR) 1 - 808 (FSR)
k_0	57 (NSR) 59 (FSR)	48 (NSR) 80 (FSR)	20 (NSR) 83 (FSR)
k_1	777 (NSR) 785 (SNPP FSR) 787 (J1 FSR)	494 (NSR) 988 (FSR)	185 (NSR) 747 (FSR)
a_1	21 (NSR) 22 (FSR)	7 (NSR) 35 (FSR)	10 (NSR) 35 (FSR)
a_2	1.0	2.0 (NSR) 0.5 (FSR)	4.0 (NSR) 0.5 (FSR)

a_3	54 (NSR) 55 (FSR)	7 (NSR) 35 (FSR)	8 (NSR) 35 (FSR)
a_4	1.0	2.0 (NSR) 0.5 (FSR)	4.0 (NSR) 0.5 (FSR)

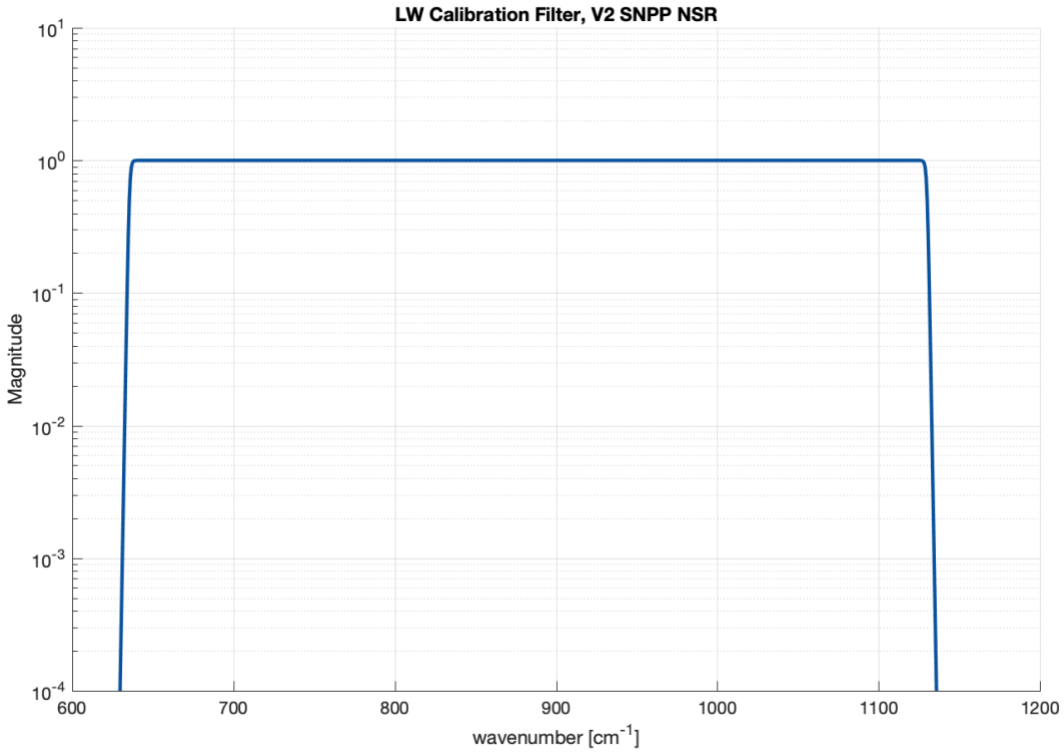

Figure 3.6.5- 1. Calibration filter for LW band (SNPP, NSR).

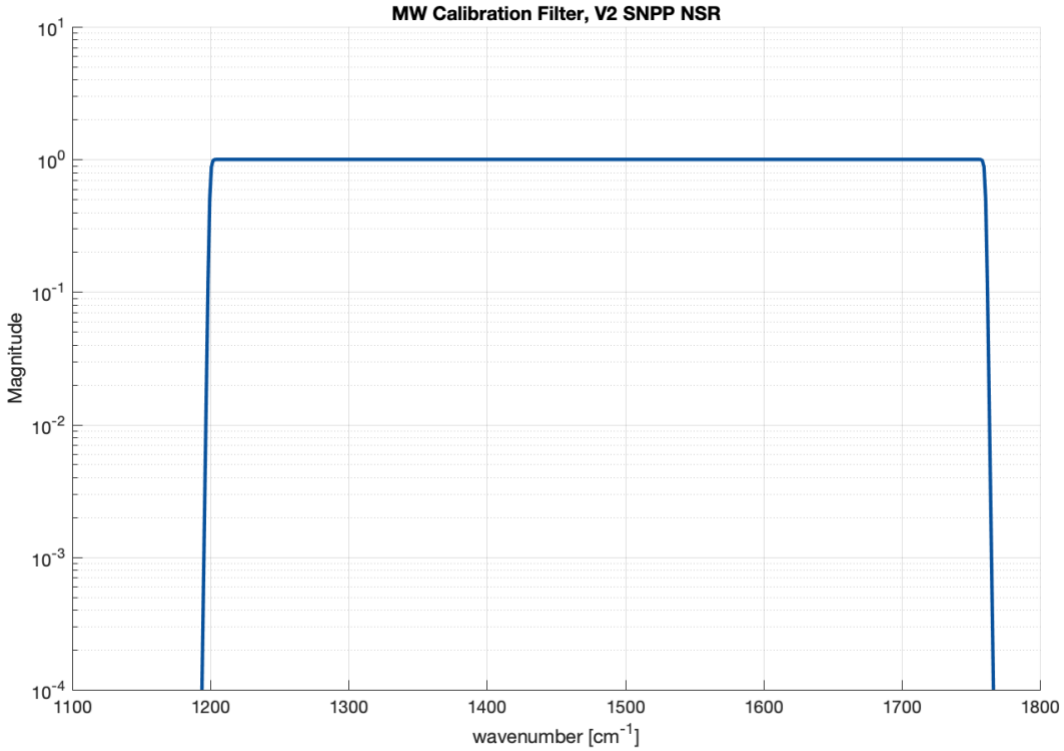

Figure 3.6.5- 2. Calibration filter for MW band (SNPP, NSR).

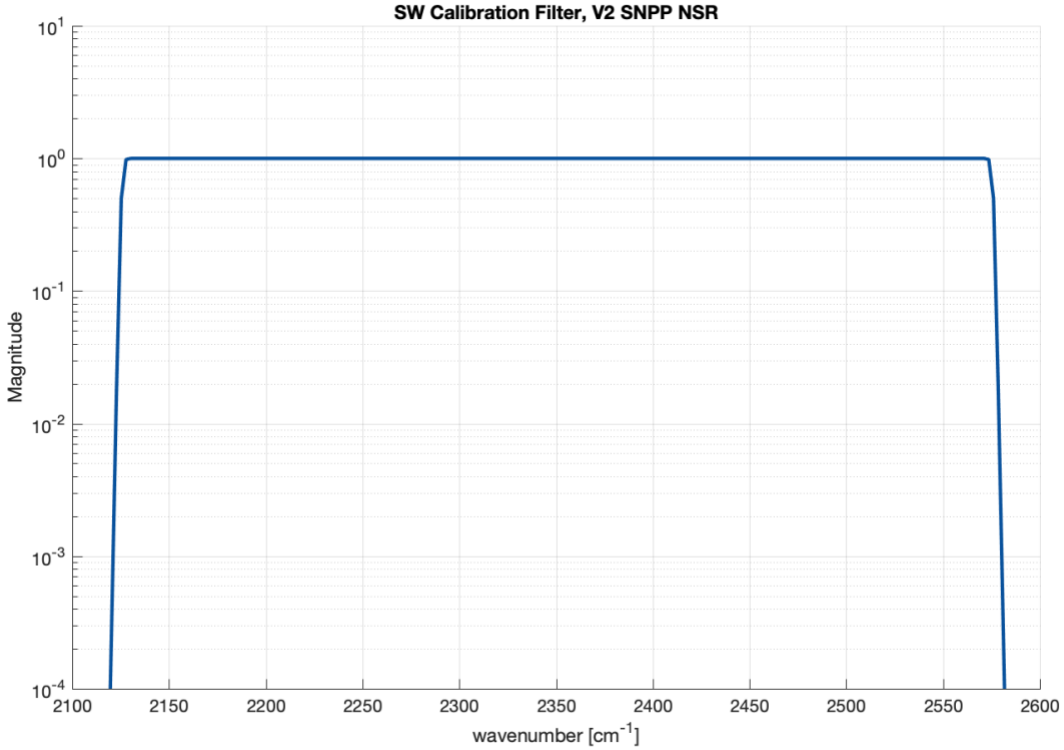

Figure 3.6.5- 3. Calibration filter for SW band (SNPP, NSR).

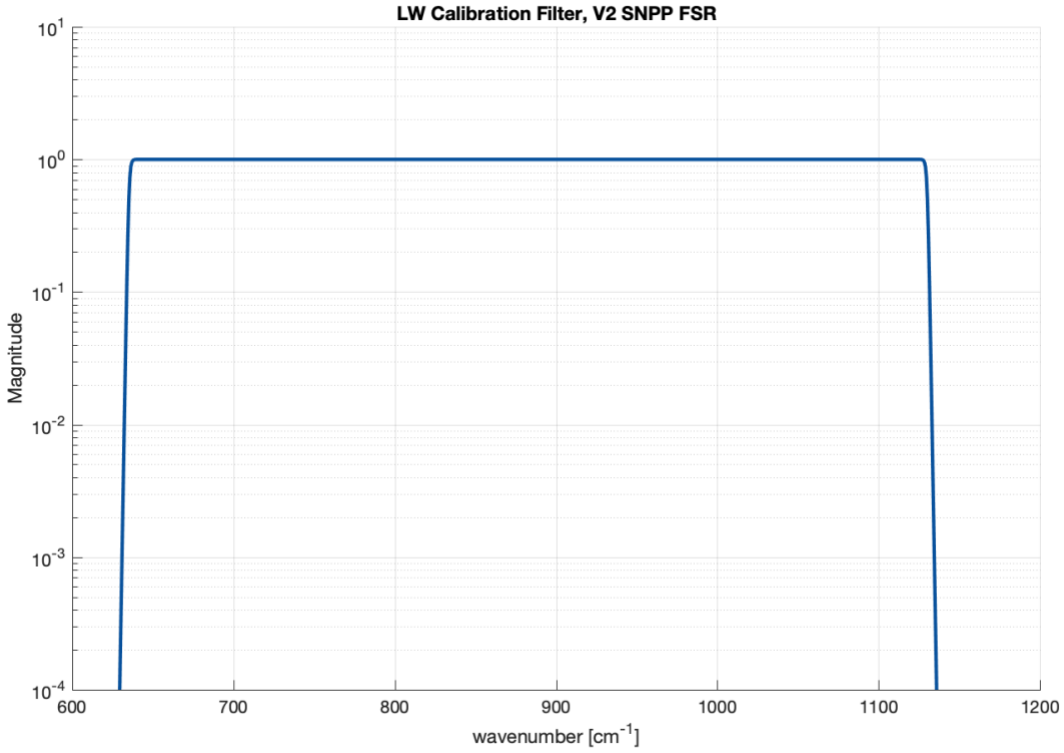

Figure 3.6.5- 4. Calibration filter for LW band (SNPP, FSR).

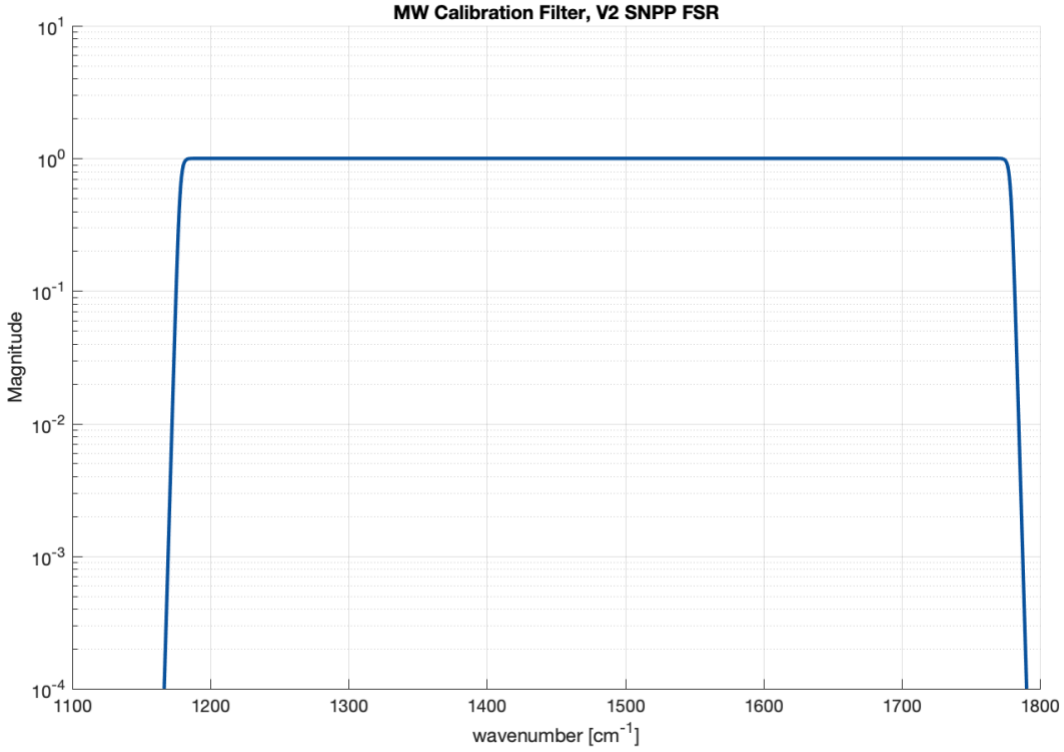

Figure 3.6.5- 5. Calibration filter for MW band (SNPP, FSR).

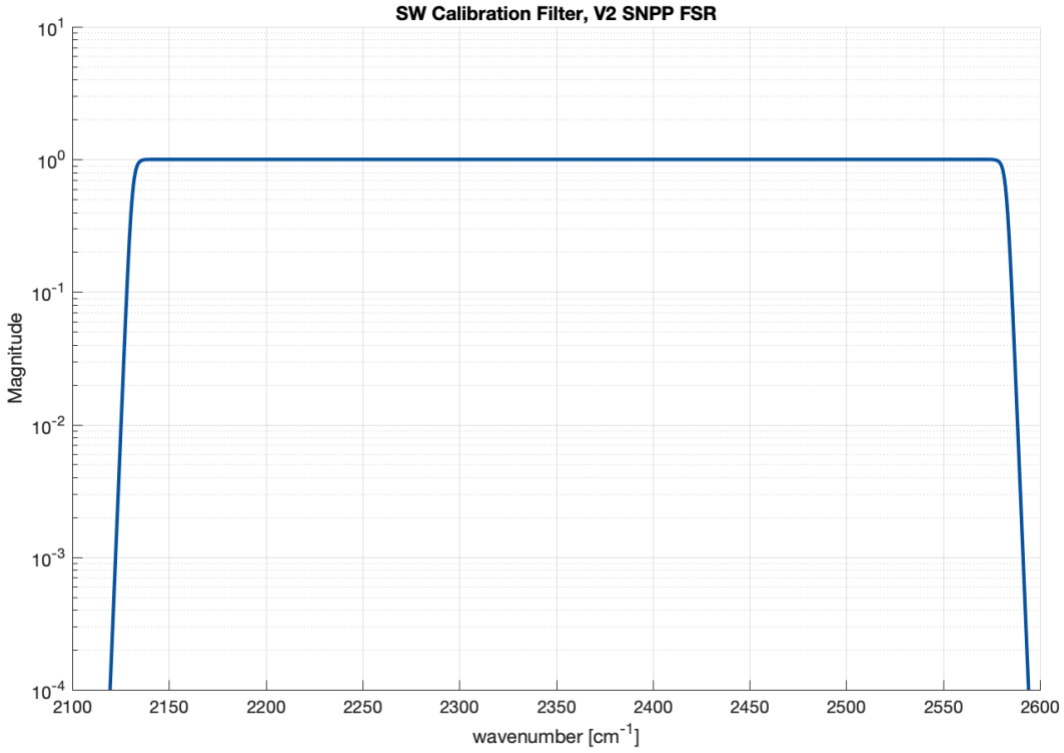

Figure 3.6.5- 6. Calibration filter for SW band (SNPP, FSR).

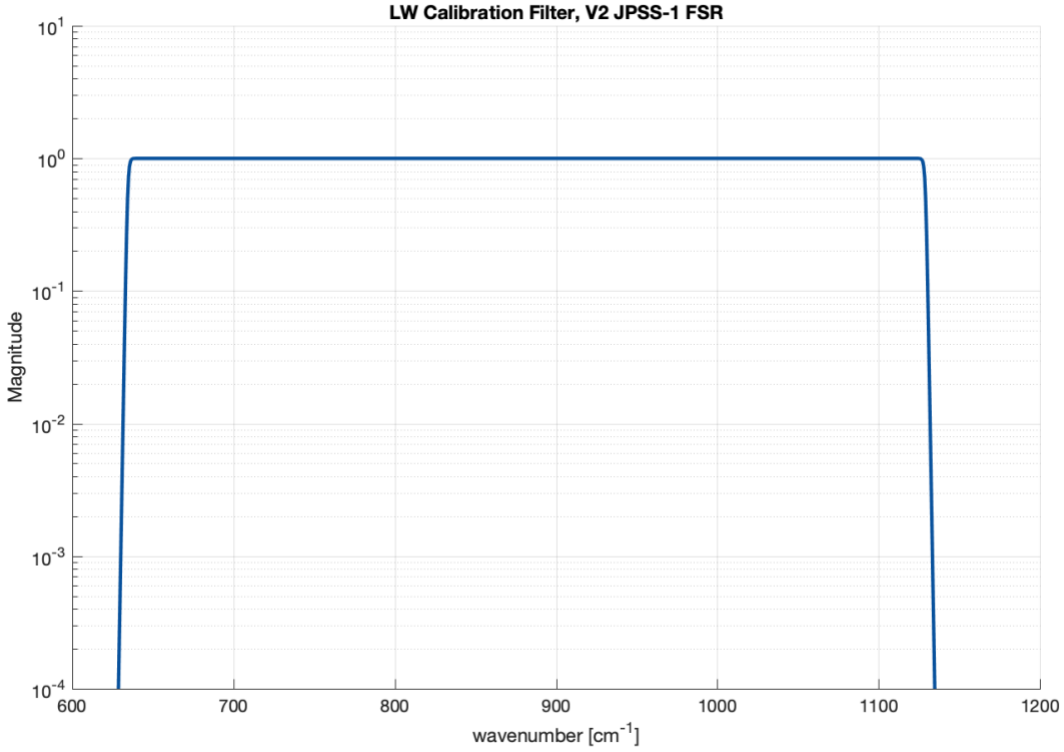

Figure 3.6.5- 7. Calibration filter for LW band (J1, FSR).

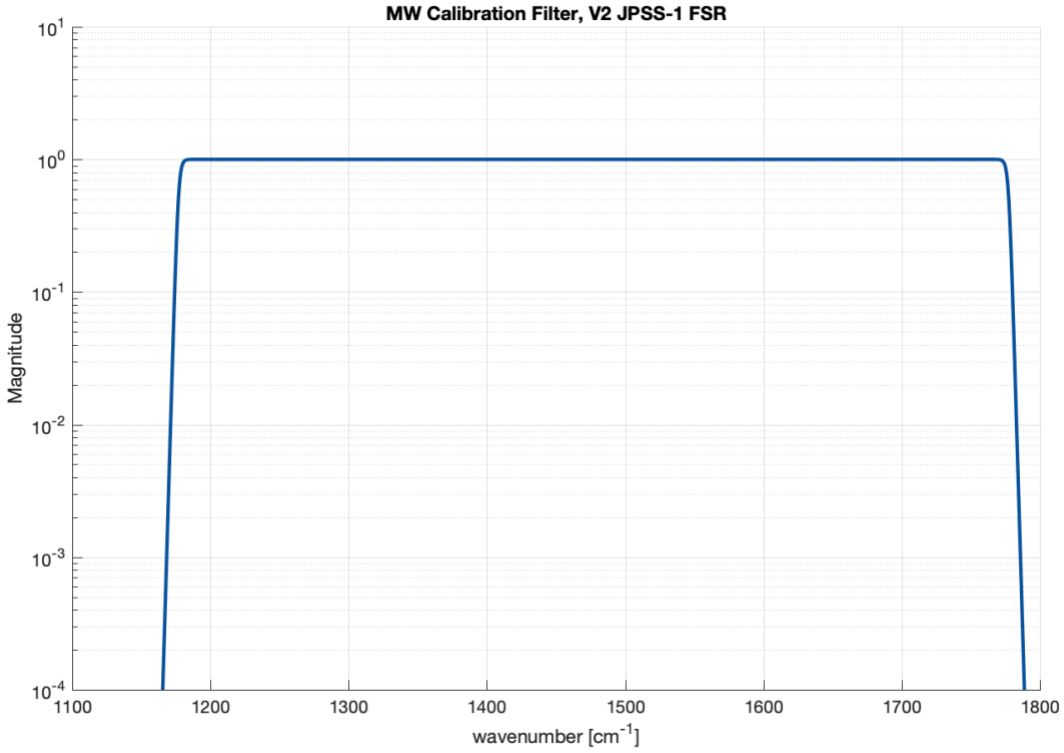

Figure 3.6.5- 8. Calibration filter for MW band (J1, FSR).

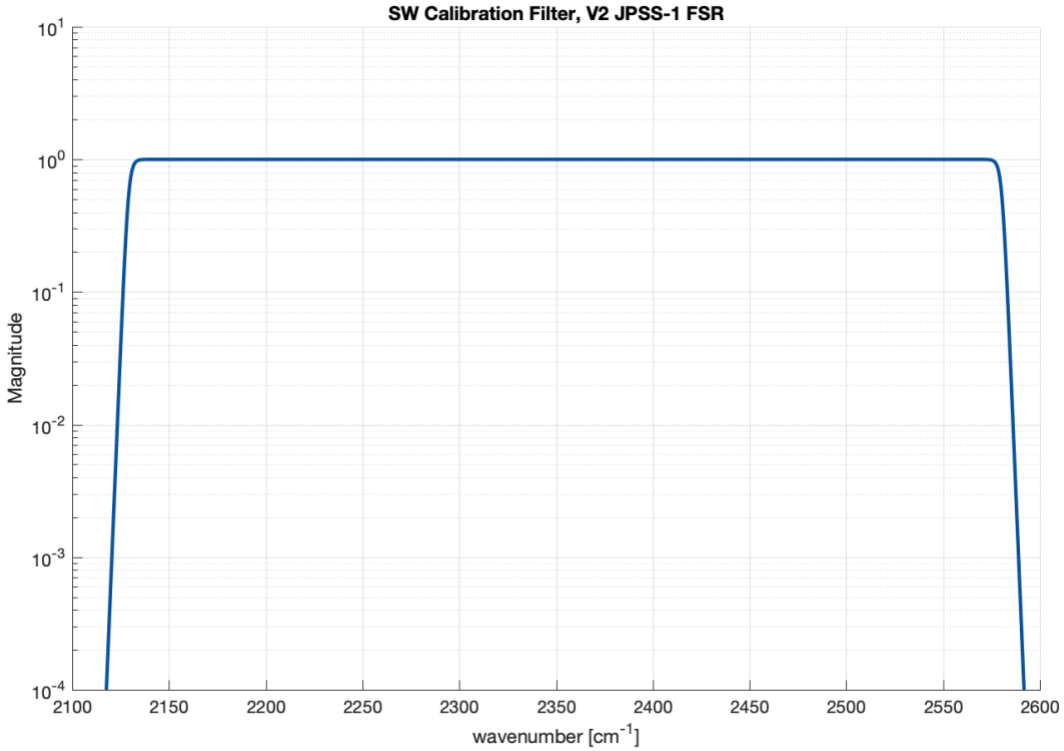

Figure 3.6.5- 9. Calibration filter for SW band (J1, FSR).

3.6.6 ILS Retrieval

The spectral calibration of the instrument is impacted by optical alignments and FOV geometry (FOV size, shape, geometry and off-axis angles). The ILS retrieval process has been designed to identify the FOV dependent parameters required to construct inverse self-apodization matrices that provide optimal correction of the self-apodization of all 27 detector channels.

The process utilizes knowledge of the FOV size, shape, geometry and off-axis angles for each FOV obtained from instrument design and instrument characterization (conducted during TVAC and on-orbit).

3.7 Signal Apodization

Unapodized radiances are output for the standard L1B product.

3.7.1 Unapodized Channel Response Function

No change.

3.7.2 Hamming's Filter Function

The spectral operators (bandguard filter, spectral resampling, self-apodization removal, and Hamming apodization are not combined into a single CMO matrix.

3.7.3 Blackman-Harris's Apodization Function

No change.

3.8 CMO Updates

The spectral operators (bandguard filter, spectral resampling, self-apodization removal, and Hamming apodization are not combined into a single CMO matrix.

3.9 Doppler Shift Correction

The Earth velocity and the satellite velocity both contribute to the relative velocity between the Earth observation and the observing instrument. The Doppler velocity is the dot product of the relative velocity vector and the unit line of sight vector and results in a spectral shift of the observations referred to as Doppler shift. Since the maximum along-track viewing angle with respect to nadir is typically very small for a cross-track scanning low Earth orbiting satellite, it is typically assumed that the Doppler shift associated with the velocity of the satellite will be negligible. However, the satellite velocity is more than an order of magnitude greater (roughly 16x for CrIS) than the maximum Earth rotation velocity at the equator, and the Doppler shift due to the satellite velocity can be shown to be significant even for very small along-track viewing angles (~1°). Furthermore, unlike the Earth rotation velocity, the satellite velocity does not have a strong latitude dependence, and the Doppler shift associated with the satellite velocity and along-track viewing angle is the dominant source of Doppler shift for high latitudes.

A physical model for the Doppler shift of the observations due to both Earth rotation and satellite velocity for the CrIS instrument was developed and tested. A module to perform Doppler shift correction has been integrated into the CrIS L1B calibration and supports three options for Doppler shift correction of the CrIS observations: no correction, correction for Doppler shift due to Earth velocity only, and full correction for Doppler shift due to Earth rotational velocity and satellite velocity. Version 3 of the CrIS NASA L1B product includes a correction for Doppler shift due to Earth rotational velocity. Full correction for Doppler shift due to both Earth rotation and satellite velocity is scheduled for inclusion in a future product release. Implementation of the full Doppler shift correction (for both satellite velocity and Earth rotation) may require a reassessment of and updates to the on-orbit focal plane array geometry and ILS parameters.

The satellite's velocity vector in ECEF (Earth-Centered, Earth-Fixed) coordinates includes both the satellite's orbital motion and a westward component due to relative motion resulting from Earth's rotation. Thus, taking the dot product of satellite velocity with the unit line of sight vector yields the total Doppler velocity $\left(v_{Doppler}\right)$. The Earth-only Doppler velocity $\left(v_{Doppler}^{Earth}\right)$ is computed separately by considering only the latter component of satellite velocity, which can be computed from the satellite position. The fractional Doppler shift $\left(\Delta\sigma_{Doppler}/\sigma\right)$ is defined as the respective Doppler velocity (Earth-only or total) divided by the speed of light c.

The DS and ICT spectra do not need to be corrected for Doppler shift since the ICT is within the instrument and the DS spectra are a measurement of the instrument background and deep space. Therefore, the Doppler shift correction should ideally be applied only to the Earth scene spectra after self-apodization removal. However, the order of operations in the calibration equation has been optimized to reduce channel-to-channel spectral ringing effects and changing the order of calibration operations is not desirable. Applying the Doppler shift correction within the sensor to user grid resampling of the numerator in the calibration equation is simplest for implementation. While the numerator is composed of a combination of ES, ICT, and DS views, applying the Doppler correction to the numerator rather than only the ES spectra has been proven to have a negligible impact on the calibrated radiances.

The fractional Doppler shift $\left(\Delta\sigma_{Doppler}/\sigma\right)$ is independent of the frequency of the channel and the effect of the Doppler shift is that the measured spectrum is stretched or shrunk to a new frequency σ' from σ:

$$\sigma' = \sigma\left(1 + \frac{\Delta\sigma_{Doppler}}{\sigma}\right)$$

Including Doppler shift correction during resampling from sensor to user grid is accomplished simply by scaling the sensor sampling interval $\Delta\sigma$ and on-axis sensor wavenumber scale by $1-\left(\Delta v/v\right)$ prior to calculation of the resampling operator.

3.10 Weak Cosine Apodization of Interferograms

For the FSR product, a very weak cosine-tapered (Tukey) window function is applied to the interferograms prior to conversion to spectra. A cosine-tapered window can be regarded as a boxcar window of width $N-2q$ points, that has a cosine roll-off spanning q appended to each end. An example of the cosine taper portion of the cosine-tapered window function, shown in the optical path difference region near positive maximum optical path difference (MOPD) is shown in Figure 3.10-1.

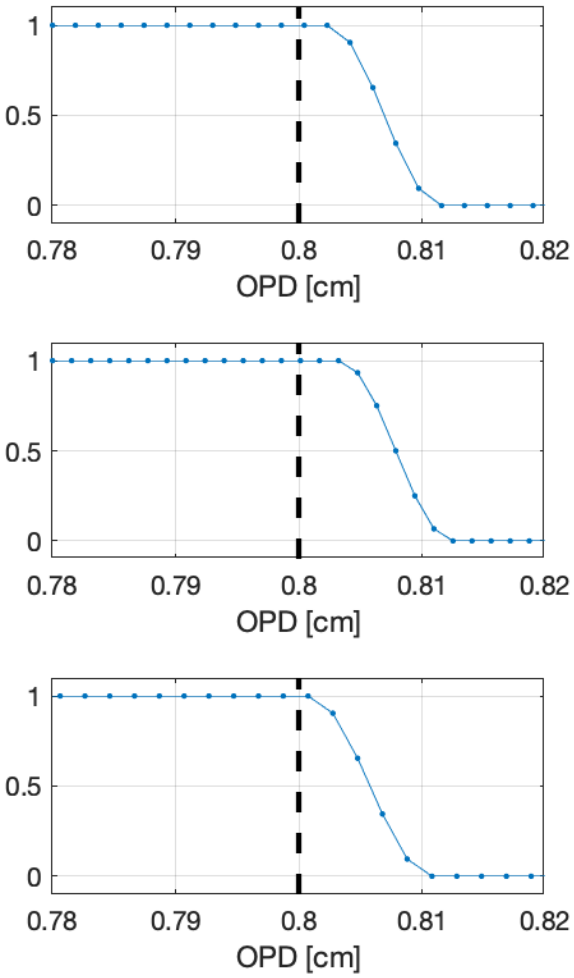

Figure 3.10- 1. An example of the cosine taper portion of the cosine-tapered window function, shown in the optical path difference region near positive MOPD is shown for the longwave (top), midwave (middle), and shortwave (bottom) bands.

This application of the very weak Tukey window function reduces the point-to-point spectral ringing that is typically associated with the Fourier transform of an interferogram with a finite MOPD and non-zero signal near MOPD. A few extra interferogram points are collected beyond the MOPD needed to meet the FSR output resolution requirements. Given these extra points, the width of the cosine roll-off can be limited to only a few points at the ends of the sensor interferogram such that the unapodized portion of the interferogram corresponds to an MOPD that is still larger than the user grid MOPD. Accordingly, the sensor grid spectral resolution, including the impact of the very weak Tukey apodization, is still finer than the unapodized user grid (output) spectral resolution. Given this consideration, the ringing behavior can be improved without impacting the unapodized output spectral resolution.

4 SPECTRAL CALIBRATION

4.1 Neon-lamp as a Spectral Reference

No change.

4.1.1 Wavelength Calculation

No change.

4.1.2 Calculation of Laser Metrology Wavelength

No change.

4.1.3 Rejecting Bad Neon Count Measurements (Quality Control)

No change.

4.2 Metrology Wavelength Monitoring

No change.

5 RADIOMETRIC CALIBRATION

5.1 Basic Radiometric Relations

No change.

5.2 General Calibration Equation

No change.

5.3 CrIS Specific Calibration Equation

The CrIS specific calibration equation, as implemented by the NASA L1B CrIS processing, using notation consistent with Section 5.3 of the CrIS SDR ATBD, is written:

$$L^{S}_{b,p,d} = L^{H} \cdot \frac{F_b \cdot f_b \cdot SA^{-1}_{b,p} \cdot f_b \cdot \left[\frac{\Delta S_1}{\Delta S_2} \left| \Delta S_2 \right| \right]}{F_b \cdot f_b \cdot SA^{-1}_{b,p} \cdot f_b \cdot \left| \Delta S_2 \right|} \quad [5.3.1]$$

$$\Delta S_1 = \left(\tilde{S}^{S}_{b,p,d} - \left\langle \tilde{S}^{C}_{b,p,d} \right\rangle \right) \quad [5.3.2]$$

$$\Delta S_2 = \left(\left\langle \tilde{S}^{H}_{b,p,d} \right\rangle - \left\langle \tilde{S}^{C}_{b,p,d} \right\rangle \right) \quad [5.3.3]$$

where,

$L^{S}_{b,p,d}$ is the calibrated scene radiance

$\tilde{S}^{S}_{b,p,d}$ are the complex uncalibrated Earth scene spectra as measured by the instrument,

$\tilde{S}^{C}_{b,p,d}$ are the complex uncalibrated cold reference (Deep Space) spectra as measured by the instrument (complex),

$\tilde{S}^{H}_{b,p,d}$ are the complex uncalibrated hot reference (ICT) spectra as measured by the instrument (complex),

L^{H} is the calculated radiance for the hot calibration reference (the ICT), calculated on the user wavenumber scale

F_b is the spectral resampling matrix operator,

f_b is the band calibration filter matrix operator,

$SA^{-1}_{b,p}$ is the Self Apodization removal matrix operator,

b, p, and d denote band, field of view, and sweep direction dependence, respectively.

For reference, the CrIS specific calibration Eq. 72 presented in the CrIS SDR ATBD is included here:

$$L^S = F_{INT}^{-1} \cdot \left[\frac{\tilde{S}^S - \langle \tilde{S}^C \rangle}{\langle \tilde{S}^H \rangle - \langle \tilde{S}^C \rangle} \right] \cdot F_{INT} L^H + F_{INT}^{-1} \cdot \left[\frac{\langle \tilde{S}^H \rangle - \tilde{S}^S}{\langle \tilde{S}^H \rangle - \langle \tilde{S}^C \rangle} \right] \cdot F_{INT} L^C \qquad [5.3.4]$$

As noted in the CrIS SDR ATBD, during normal on-orbit operation the cold reference radiance $L_C = 0$ so that the second term in equation [5.3.4] can be ignored resulting in a further simplification:

$$L^S = F_{INT}^{-1} \cdot \left[\frac{\tilde{S}^S - \langle \tilde{S}^C \rangle}{\langle \tilde{S}^H \rangle - \langle \tilde{S}^C \rangle} \right] \cdot F_{INT} L^H \qquad [5.3.5]$$

In the CrIS SDR ATBD implementation, the F_{INT}^{-1} term in equation [5.3.4] is combined into the CMO (Correction Matrix Operator) matrix. The CrIS SDR ATBD as defines the CMO matrix:

$$CMO_{b,p} = H_b \cdot R_{b,p}^{-1} \cdot SA_{b,p}^{-1} \cdot F_b \cdot f_b \qquad [5.3.6]$$

where,

H_b is the Hamming apodization matrix operator, and

$R_{b,p}^{-1}$ residual ILS removal matrix operator.

Omitting the Hamming apodization and residual ILS removal from [5.3.6], the CrIS SDR ATBD CrIS specific calibration equation (Eq. [5.3.5]) can be rewritten in a form that can be more easily compared with the NASA L1B CrIS Calibration Equation [5.3.1]:

$$L^S = SA_{b,p}^{-1} \cdot F_b \cdot f_b \cdot \left[\frac{\tilde{S}^S - \langle \tilde{S}^C \rangle}{\langle \tilde{S}^H \rangle - \langle \tilde{S}^C \rangle} \right] \cdot F_{INT} L^H \qquad [5.3.7]$$

5.4 ICT Radiometric Model

No change.

5.4.1 Radiometric Error

No change.

5.4.2 Radiometric Model Formulation

The ICT radiometric model is calculated on the user wavenumber grid. Accordingly, the spectrally resolved parameters in SDR ATBD Table 14 are on the user wavenumber grid.

The J1 Internal Calibration Target (ICT) has much higher emissivity than the SNPP ICT. In addition, the J1 ICT is a specular trap while the SNPP ICT is a diffuse cylindrical cavity. Equations 74a through 78c are used for the radiometric model of both ICT designs, but view factors are sensor dependent. All of the view factors, except for the view to the cold beamsplitter, for the J1 ICT radiometric model are set to zero. Replace Table 15 in the reference ATBD with Table 5.4.2-1 below.

Table 5.4.2- 1. Fraction of view from ICT bottom surface to each environment surface (notional).

View from	To	SNPP Fractional View to Environment	J1 Fractional View to Environment
ICT Base	ICT Walls	-	-
ICT Base	ICT Base	-	-
ICT Base	ICT Baffle	0.175	0
ICT Base	Scan Baffle	0.508	0
ICT Base	Frame	0.214	0
ICT Base	Opto-Mechanical Assembly		
ICT Base	Warm Beamsplitter	0.086	0
ICT Base	Cold Beamsplitter	0.008	1
ICT Base	Space	0.009	0

5.5 ICT Temperature Computation

No change.

5.6 Signal Coaddition

N^{ma} = 29 for the DS and ICT signal coaddition.

5.6.1 Moving Average

The Earth Scene (ES) views in each scan line are calibrated using reference Deep Space (DS) and Internal Calibration Target (ICT) views from the current and adjacent scan lines if they are available. In the optimal situation, reference views from the 14 preceding scan lines and the 14 following scan lines will be used, in addition to the reference views from the current scan line. However, the calibration will still be performed if as few as one reference view of each type is

available. If a calibration is performed with fewer than the optimal number of reference views, for example due to a data drop-out or an instrument change, the noise in the calibrated ES spectra will be elevated. If there are 24 or more views in the moving average, the radiometric calibration quality flag will be set to 'No issues detected' (value = 0), if there are between 19 and 24 views in the moving average, the radiometric calibration quality flag will be set to 'good' (value = 1), and if there are 19 or fewer views in the moving average, the radiometric calibration quality flag will be set to 'invalid' (value = 2).

5.6.2 Impact of Temperature Drift

No change.

5.6.3 Throughput Delay

No change.

6 GEOMETRIC CALIBRATION

The NASA L1B software includes a new geolocation implementation based on the approach outlined in the CrIS SDR ATBD and the VIIRS SDR Geolocation ATBD. The CrIS SDR ATBD describes the sensor dependent portion of geolocation (line of sight vector calculation from instrument telemetry) and the VIIRS SDR ATBD describes the sensor independent part (earth location from sensor line of sight).

L1B geolocation fields are additionally adjusted to account for terrain. This is done using the approach described in the VIIRS SDR ATBD (which applies to VIIRS SDRs but not CrIS SDRs). The digital elevation model (DEM) used for L1B terrain correction and field-of-view geography (see below) is the equal-angle 30 arcsecond model made available as part NASA's SDP toolkit. For latitudes beyond +/- 70 degrees, the DEM has been resampled to a pair of azimuthal equal-area projections at 1 km resolution covering the north and south poles.

The L1B product includes a number of geolocation fields beyond those provided in SDR geolocation. A brief outline on how a number of these fields are derived is provided below.

Field of View Extent and Geography

lat_bnds, lon_bnds, land_frac, surf_elev, surf_elev_sdev

The L1B product includes for each observation a series of 8 locations that describe the perimeter of the FOV's intersection with the earth's surface, accounting for terrain. These are based on the longwave FOV angular diameter values that come from the CrIS engineering packet. (All other FOV-specific constants used for geolocation reference the longwave values, consistent with the CrIS SDR ATBD.)

The angular diameter values are further used to find points from the DEM that are within the spatial extent of the observation, which are then aggregated to provide land fraction and surface elevation statistics. Testing each DEM point for inclusion is done via a dot product threshold test between the satellite to FOV center vector and satellite to DEM point vector.

Sun Glint

sun_glint_lat, sun_glint_lon, sun_glint_dist

Glint location is calculated in the L1B product using the WGS84 earth model ellipsoid. The glint location is first estimated using a spherical earth model by identifying the position along the great circle arc connecting the subsatellite and subsolar points where the satellite and solar zenith angles are equal (as required for specular reflection of sunlight). This initial approximation is then refined using an iterative procedure that ensures the reflection of sunlight off the ellipsoid surface at the glint location is directed toward the spacecraft to within an angular tolerance of 0.001 degrees.

Orbital information

asc_node_tai93, asc_node_lon, asc_node_local_solar_time, mean_anom_wrt_equat, solar_beta_angle

Spacecraft ephemeris information is used in L1B geolocation to estimate orbital parameters for

use with the SGP4 simplified perturbations model. Currently a single ephemeris sample for each granule is used to perform a fixed-point iteration [Montenbruck2000] to derive the model parameters. A future implementation may incorporate more ephemeris samples.

Once model parameters have been established, the SGP4 propagator is used to determine the time, longitude, and local solar time of the most recent equator crossing. Orbit phase (mean_anom_wrt_equat) is calculated based on time elapsed since the equator crossing and the mean motion orbital parameter. Solar beta angle is calculated with respect to the orbital plane described via the inclination and ascending node orbital parameters.

6.1 Coordinate Systems

No change.

6.1.1 Coordinate System Definition

No change.

6.1.2 Interferometer Optical Axis Reference (IOAR)

No change.

6.1.3 Rotating Mirror Frame (RMF)

No change.

6.1.4 Scene Selection Mirror Mounting Feet Frame (SSMF)

No change.

6.1.5 Scene Selection Module Reference (SSMR)

No change.

6.1.6 Instrument Alignment Reference (IAR)

No change.

6.1.7 Spacecraft Body Frame (SBF)

No change.

6.1.8 Orbital Coordinate System (OCS)

No change.

6.1.9 Earth Centered Inertial (ECI)

No change.

6.1.10 Earth Centered Earth Fixed (ECEF) or Earth Centered Rotating (ECR)

No change.

6.1.11 World Geodetic System 1984 (WGS84)

No change.

6.1.12 Topocentric-Horizon Coordinate System (THCS)

No change.

6.2 Coordinate System Transformations

No change.

6.3 Algorithm Partitioning

No change.

6.4 Sensor Specific Algorithm

No change.

6.4.1 CrIS FOV LOS in SSMF Coordinate System

No change.

6.4.2 SSMF to SBF Transformation Operator

No change.

6.4.3 CrIS FOV LOS in SBF Coordinate System

No change.

6.5 Spacecraft Level Algorithm

No change.

6.6 Timing Conventions

No change.

7 MODULES DEFINITION

This section summarizes the key processing steps necessary to transform L1A into L1B. The overall processing chain can be partitioned into modules listed below.

1. Initialization
   - Software initialization, the algorithm needs a one-time initialization
2. Input Data Handling
   - Low level and configuration data handling for software
   - Calibration and science data handling
3. Preprocessing
   - Interferogram to spectrum transformation
   - Moving average handling
   - Non-Linearity Correction
   - FCE detection and correction
4. Spectral Calibration
   - Laser wavelength calibration from neon lamp data
   - Laser wavelength drift monitoring
   - Spectral axis labeling and alias unfolding
5. Radiometric Calibration
   - ICT radiance calculation
   - Complex calibration (removes instrument induced offset and phase)
   - Polarization correction (not included in v2.0, will be included in a future release)
   - Spectrum correction (correct for ILS, calibration filter, and resample to a fixed wavenumber grid)
6. Geolocation
   - FOV LOS calculation relative to spacecraft body frame
7. Quality Control
   - NEdN estimation
   - Metrology wavelength monitoring
   - Temperatures monitoring
   - Lunar intrusion detection
   - Imaginary radiance threshold tests
8. Post-processing
   - User required spectral bins selection
   - SDR data formatting
9. Output Data Handling

The conventions used in the flowcharts shown in this section are described in Figure 7.0-1.

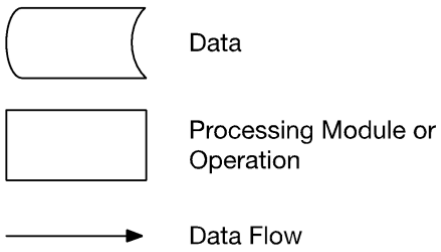

Figure 7.0- 1. Conventions used in the flowcharts included in this section.

The overall processing chain required to transform raw interferograms into spectrally and radiometrically calibrated and corrected spectra is shown in Figure 7.0-2 and Figure 7.0-3. This replaces Figure 59 in the CrIS SDR ATBD.

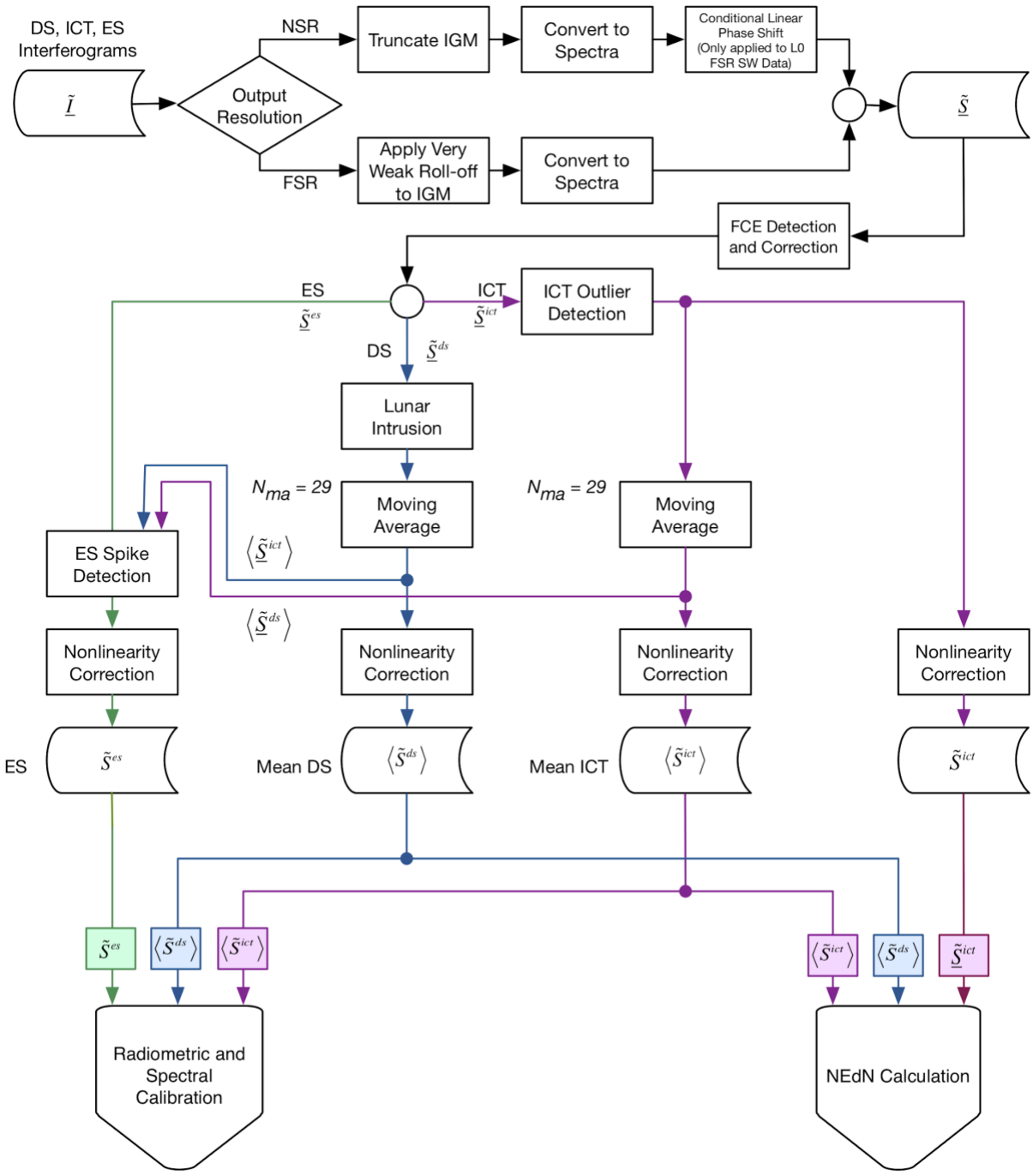

Figure 7.0- 2. General flow diagram for operations performed prior to radiometric and spectral calibration.

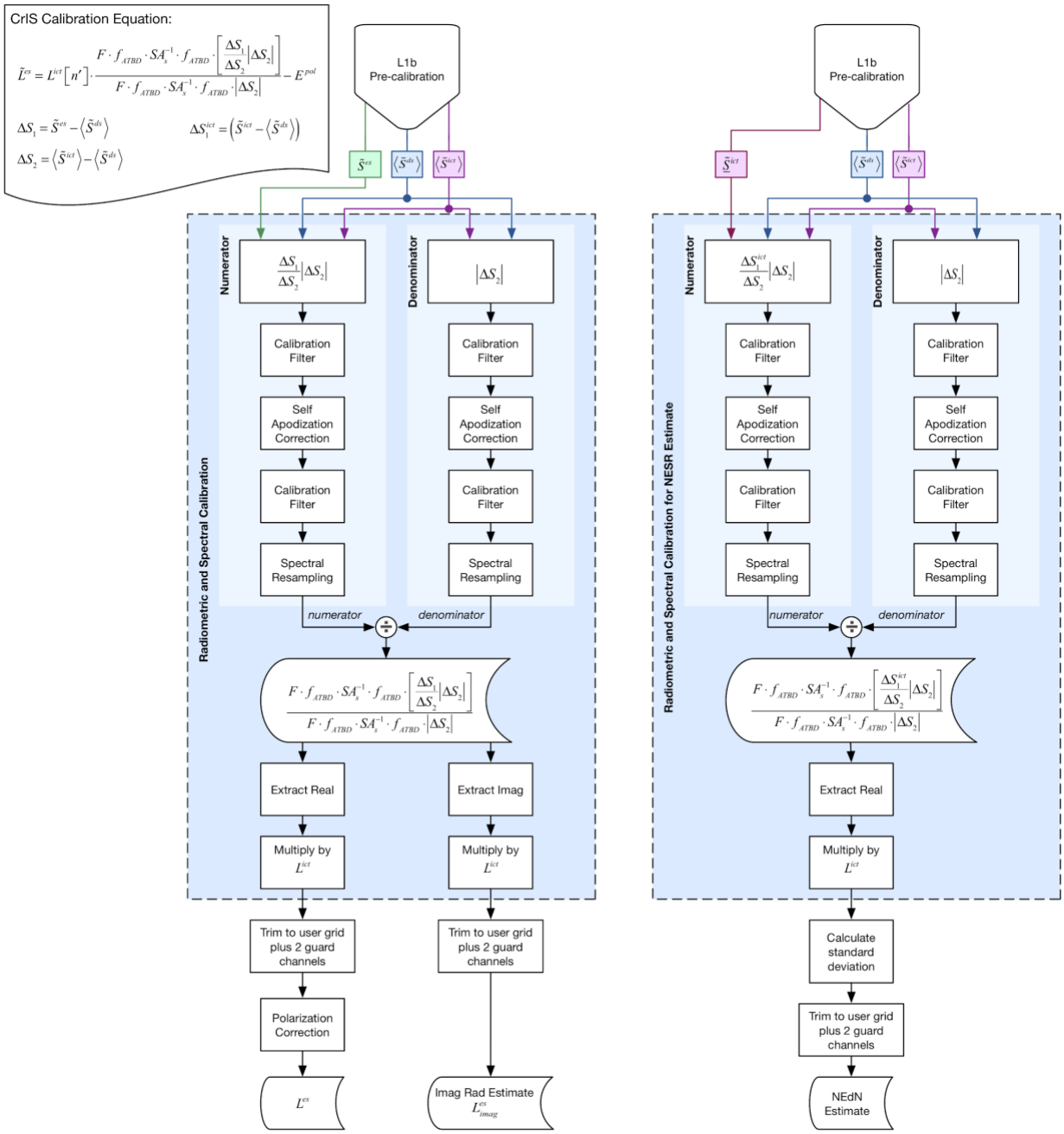

Figure 7.0- 3. General flow diagram for the radiometric and spectral calibration (full calibration is used for NEdN estimates). Doppler correction is performed within the resampling operator.

7.1 Initialization

The ILS curve fit parameters in the CrIS SDR ATBD (Table 17), which are intended for correction of modulation efficiency variation with OPD, are not applicable to the NASA L1B processing.

The configuration options in the CrIS SDR ATBD (Table 18: Tunable Parameters Provided via Configuration Files) that modify the processing performed by the CrIS SDR algorithm are not

applicable to the NASA L1B processing. The instrument parameters that are configured within the L1B processing are listed in Table 7.1-1.

Table 7.1- 1. Parameters defined in L1B processing package.

L1B mnemonic	Description
sensor.Rf	Decimation factor
sensor.An	Alias number
sensor.N	Number of points in sensor grid interferogram
sensor.iflip	spectral unfolding index
sensor.FOVangle	angle to center of FOV
sensor.FOVradius	FOV radius
sensor.startbit	FIR accumulator start bit
sensor.ModEff	
sensor.Vinst	nonlinearity correction Vinst values
sensor.a2_now	nonlinearity correction a2 coefficients
user.MOPD	Maximum Optical Path Difference (MOPD) corresponding to output resolution
user.output_range	spectral range for output data
FIRfilter.lw.h.real	LW FIR filter coefficients (real part)
FIRfilter.lw.h.imag	LW FIR filter coefficients (imag part)
FIRfilter.mw.h.real	MW FIR filter coefficients (real part)
FIRfilter.mw.h.imag	MW FIR filter coefficients (imag part)
FIRfilter.sw.h.real	SW FIR filter coefficients (real part)
FIRfilter.sw.h.imag	SW FIR filter coefficients (imag part)
invalidNeonCalibrationPercentageThreshold	neon calibration quality control parameter
computedWavelengthRejectionThreshold	neon calibration quality control parameter
c	calibration filter coefficients
fb	calibration filter frequency response
h	Planck constant used in ICT radiance calculation
k	Boltzmann constant used in ICT radiance calculation
c	speed of light constant used in ICT radiance calculation
orbit_time_vector	orbit times corresponding to SSM Baffle Offset model values in engineering packet

7.2 Input Data Handling

The implementation of data handling is consistent with the CrIS SDR ATBD. It is notable that the conversion of CCSDS packet data to “raw” interferogram observations, as well as science and engineering coefficients and measurements, is separated into a “CrIS L1A” telemetry conversion stage. That initial processing stage is not responsible for triggering science data processing

activities, i.e. it is a simplified model from the “operational” implementation model described in the ATBD. L0 telemetry equivalent to RDRs is converted to L1A granules represented as files; groups of L1A granule files are then used for science SDR-equivalent L1B product generation. Granulation of CrIS data is principally done in the L1A stage of processing.

7.3 Preprocessing

The introductory section is theoretically consistent with the CrIS SDR ATBD.

7.3.1 Interferogram to Spectrum Transformation

As noted in Section 2.5.2, during the first part of the SNPP mission the effective spectral resolution of CrIS data received from the satellite was lower in the short-wave and mid-wave infrared bands than in the long-wave infrared band. Level 0 data received during this initial period is referred to as Normal Spectral Resolution (L0 NSR). On 4 December 2014 (15:06 UTC), the resolution of the short-wave and mid-wave data transmitted from the SNPP satellite was increased to match the long-wave resolution. Level 0 data received from this time through 2 November 2015 (15:48 UTC) is referred to as Full Spectral Resolution (L0 FSR). On 2 November 2015 (16:06 UTC), the satellite began transmitting long-wave and short-wave interferograms with extra points on the ends. Level 0 data received from this time forward is referred to as Extended Spectral Resolution (L0 XSR). For the NASA L1B SNPP product, L1B calibrated radiance datasets are produced at two different resolutions, to meet the goals of providing a spectrally consistent product with the longest possible duration and also with the highest possible spectral resolution. These L1B datasets are referred to as NSR and FSR.

CrIS data received from the J1 satellite has been at L0 XSR for the entire mission. For the NASA L1B J1 product, L1B calibrated radiances are produced only at FSR.

For the L1B NSR output, the L0 FSR and L0 XSR input interferograms are truncated to L0 NSR resolution prior to transformation to spectra. Additionally, for L1B NSR output data produced from L0 Full Spectral Resolution (L0 FSR) input data, a linear phase shift is applied to the MW band complex spectra after truncation of the full resolution interferograms to low resolution interferograms. This corrects for a linear phase shift in the MW that was introduced by the onboard processing for FSR input data. This linear phase shift is not applied for NSR or XSR L0 input. For the L1B FSR dataset, no truncation or linear phase shift is applied to the XSR L0 input.

As noted in Section 3.10, a very weak cosine-tapered (Tukey) window function is applied to the interferograms prior to conversion to spectra for the FSR product. This application of the very weak Tukey window function reduces the point-to-point spectral ringing that is typically associated with the Fourier transform of an interferogram with a finite maximum optical path (MOPD) difference and non-zero signal near MOPD. The width of the cosine roll-off is limited to only a few points at the ends of the sensor interferogram such that the unapodized portion of the interferogram corresponds to an MOPD that is still larger than the user grid MOPD and the unapodized output resolution is unaffected.

Otherwise, 7.3.1 is theoretically consistent with the CrIS SDR ATBD.

7.3.2 Moving Average Handling

This module handles the moving average of calibration target measurements (DS, ICT). Unlike the NOAA SDR algorithm, the NASA L1B algorithm uses a moving window of 29 DS and ICT measurements (14 anterior scans, the current scan, and 14 posterior scans; temperatures and spectra) are averaged per the default setting. The moving average is calculated for each scan line, and the FIFO method described in the CrIS SDR ATBD is not used. The moving window averages for the DS and ICT are calculated using the uncalibrated spectra prior to non-linearity correction.

In the event that a fringe count error (FCE) has been detected, then the phase of the Earth scene, ICT, or DS spectra impacted by the FCE is corrected to match the phase of all the other spectra in the current granule (and anterior/posterior context granules if applicable). If verification of the FCE correction indicates that the correction has failed for an ICT or DS spectra, those spectra will be excluded from the respective moving average. If verification of the FCE correction indicates that the correction has failed for an Earth scene, then the FCE failed quality flag is asserted for that observation to indicate that the observation is invalid.

A general description of the moving window average process is given in Section 5.6.1.

7.3.2.1 Exception Handling

If any ICT or DS spectrum is declared invalid by CrIS sensor, ICT outlier test, lunar intrusion test or other QC measure, then the corresponding measurements are excluded from the moving window average.

If the number of valid spectra in the moving window drops below a threshold value (set such that the noise increase due to decreased average size in the reference view is less than 10%), then the “Degraded Radiometric Calibration” flag is set. If there are no valid spectra in the moving average window, then the “Invalid Radiometric Calibration” flag is set.

If a science telemetry packet is missing for a given 8-second sweep, then those telemetry values shall be excluded from the moving window average.

7.4 Spectral Calibration

No change. See Section 7.5.3 for Doppler correction.

7.4.1 Laser Wavelength Calibration from Neon Lamp Data

An update of metrology laser wavelength is performed for each granule based on the calibration neon count. The F-matrix resampling operator is computed separately for each granule using Neon data contained in the most coincident engineering packet. The spectral operators (calibration filter, spectral resampling, self-apodization removal) are not combined into a single

CMO matrix.

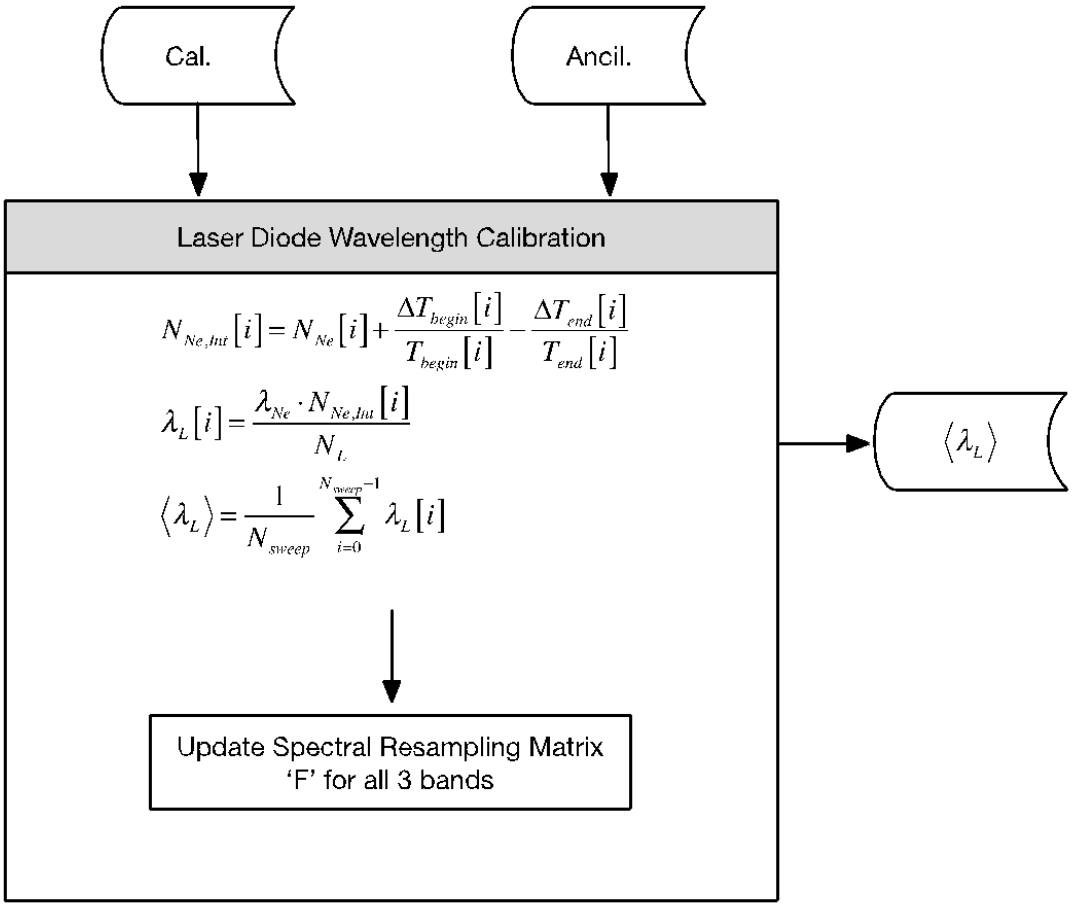

Figure 7.4.1- 1. Metrology laser wavelength calibration flowchart (replaces Figure 63 in CrIS SDR ATBD).

7.4.1.1 Definition of Variables

Calibration data from engineering packet

$N_{Ne}[i]$ integer neon fringe count from ith sweep

$T_{begin}[i]$ integer neon fringe count parameter from ith sweep used for interpolation

$T_{end}[i]$ integer neon fringe count parameter from ith sweep used for interpolation

$\Delta T_{begin}[i]$ integer neon fringe count parameter from ith sweep used for interpolation

$\Delta T_{end}[i]$ integer neon fringe count parameter from ith sweep used for interpolation

N_{sweep} Number of neon calibration sweeps collected & reported in engineering packet

N_L number of laser metrology wavelengths used to meter OPD during neon calibration sweep (N_L = 7985 always)

Ancillary data from engineering packet

λ_{Ne} reference neon wavelength (703.44835 nm)

Local variables

$N_{Ne,Int}[i]$ neon wavelengths counted during ith calibration sweep (non integer, interpolated)

Output variables

λ_L Average metrology laser wavelength computed from current engineering packet neon calibration data

7.4.1.2 Exception Handling

The averaged metrology laser wavelength is computed from many neon calibration sweeps (30 is the default). Outliers are removed before the average is re-computed and reported. See section 4.1.3 of this document and the CrIS SDR ATBD, and the NASA L1B Quality Flag Description Document for more information on outlier definition and QF assertion.

7.4.2 Laser Wavelength Drift Monitoring

This section is not applicable to the NASA CrIS L1B processing software.

7.4.3 Spectral Axis Labeling and Alias Unfolding

The spectral calibration module defines the on-axis sensor spectral grid associated with each raw spectrum (band dependent), and the output spectral grid (band dependent). Based on the latest laser diode wavelength estimate, the spectral grid spacing and the minimum wavenumber of the band are computed. The raw spectrum is then rotated by the desired number of points to unfold the spectral alias that was introduced by filtering and decimation on-board the CrIS sensor. Spectral fold points have been derived for each band. The spectral unfolding yields a continuous spectrum free of alias fold points and with channel centers defined by the metrology sampling interval λ_s^b, decimation factor DF_b and the number of complex interferogram points processed N_b.

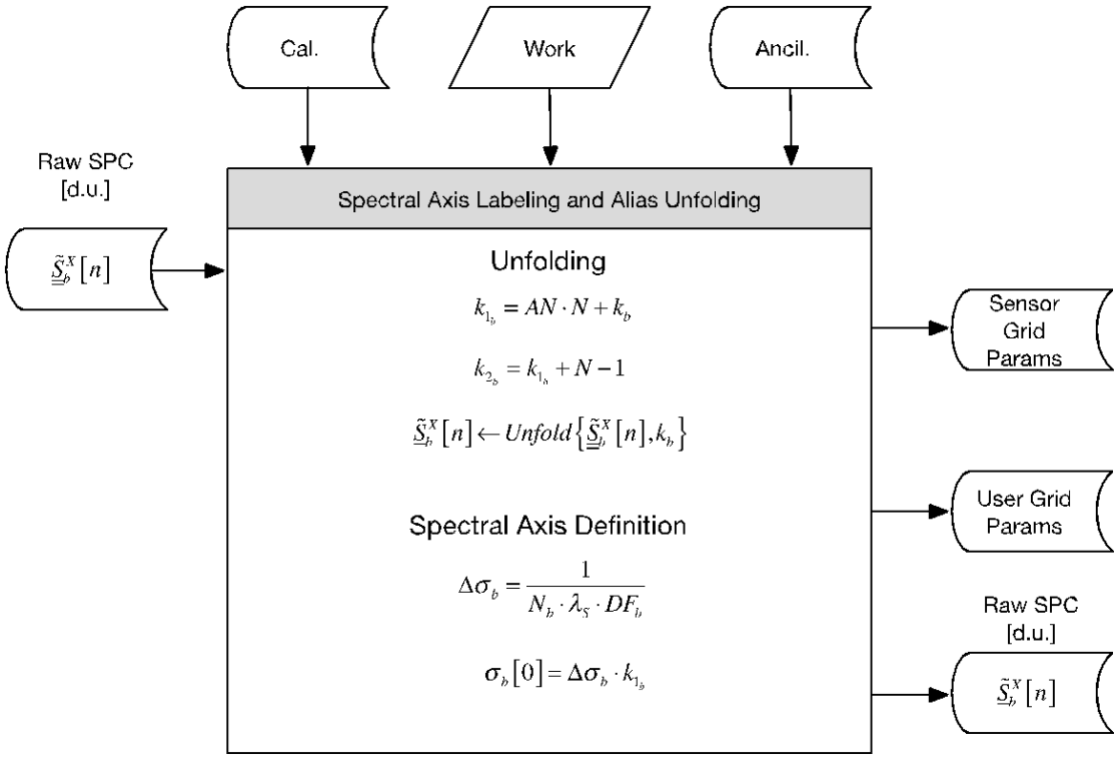

Figure 7.4.3- 1. Spectral axis labeling and aliasing unfolding.

7.4.3.1 Definition of Variables

Input variables

$\tilde{\underline{S}}_b^X[n]$ raw complex spectrum for band 'b' in [d.u.] prior to spectral unfolding, corresponding to X = DS, ICT, or ES. These spectra have not yet been through non-linearity correction.

Calibration Data

λ_S metrology sampling interval (cm) ($\lambda_s = \lambda_L/2 \approx 775x10^{-7}\,cm$). The sampling interval is half the laser metrology wavelength.

Ancillary Data

$\sigma_{0_b}^{req}$ required minimum wavenumber channel center of first channel located in the pass band of band 'b' for the L1B output spectral grid (cm^{-1}).

(LW = 650.000 cm-1, MW = 1210.000 cm-1, SW = 2155.000 cm-1)

$\sigma_{1_b}^{req}$ required maximum wavenumber channel center of last channel located in the pass band of band 'b' for the L1B output spectral grid (cm^{-1}).

(LW = 1095.000 cm-1, MW = 1750.000 cm-1, SW = 2550.000 cm-1)

DF_b decimation factor for band ‘b’

AN_b alias number for band ‘b’

k_b index to wavenumber channel to be used for spectral unfolding

Output variables

$\tilde{S}_b^X[n]$ raw complex spectrum for band ‘b’ in [d.u.] after spectral unfolding, corresponding to X = DS, ICT, or ES. These spectra have not yet been through non-linearity correction

Sensor grid parameters: including interferogram sampling interval (Δx), on-axis spectral sampling interval ($\Delta\sigma$), on-axis spectral sampling grid (σ), and required minimum/maximum wavenumber channel center of first/last channel located in the pass band of band ‘b’ for the L1B output spectral grid ($\sigma_{0_b}^{req}, \sigma_{1_b}^{req}$)

User grid parameters: including interferogram sampling interval (Δx), on-axis spectral sampling interval ($\Delta\sigma$), on-axis spectral sampling grid (σ)

Operators

$Unfold\{V[n], k_b\}$ shifts a complex numerical vector V according to a fold point k_b

7.4.3.2 Exception Handling

None.

7.5 Radiometric Calibration

The CrIS specific calibration equation, as implemented by the NASA L1B CrIS processing, using notation consistent with CrIS SDR ATBD, is provided in Equation [7-5-a].

[7.5-a]

$$\tilde{L}_{b,p,d}^{es}[n'] = L_b^{ict}[n'] \cdot \frac{F[n,n'] \cdot f_{ATBD}[n] \cdot SA_s^{-1} \cdot f_{ATBD}[n] \cdot \left[\frac{\Delta S_1}{\Delta S_2}|\Delta S_2|\right]}{F[n,n'] \cdot f_{ATBD}[n] \cdot SA_s^{-1} \cdot f_{ATBD}[n] \cdot |\Delta S_2|} - E_{b,p,i}^{pol}[n']$$

[7.5-b]

$$\Delta S_1 = \left(\tilde{S}_{b,p,d}^{es}[n] - \left\langle \tilde{S}_{b,p,d}^{ds}[n] \right\rangle\right)$$

[7.5-c]
$$\Delta S_2 = \left(\left\langle \tilde{S}^{it}_{b,p,d}\left[n\right] \right\rangle - \left\langle \tilde{S}^{ds}_{b,p,d}\left[n\right] \right\rangle \right)$$

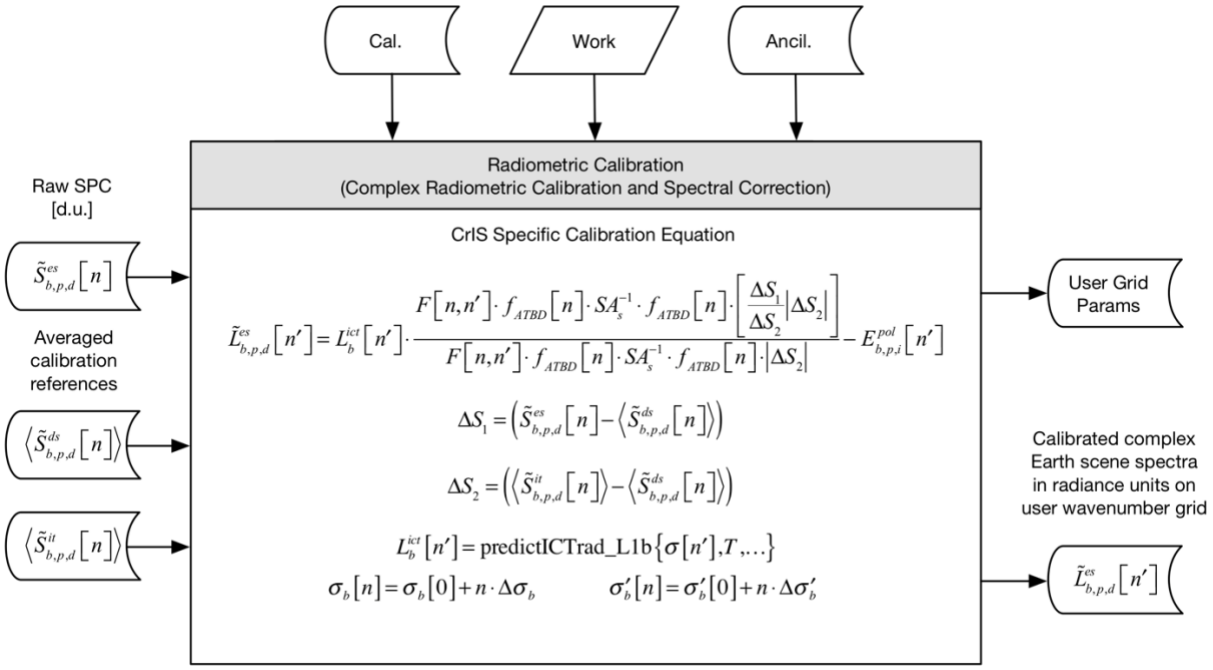

Figure 7.5- 1. CrIS radiometric and spectral calibration.

Definition of Variables

Input Variables

$\tilde{S}^{es}_{b,p,d}\left[n\right]$ complex uncalibrated Earth scene spectra, expressed in [d.u.] at channel center "n", prior to nonlinearity correction. Uncalibrated instrument counts for nth channel on sensor wavenumber grid for FOV "p", sweep direction "d" and band "b"

$\left\langle \tilde{S}^{ds}_{b,p,d}\left[n\right] \right\rangle$ complex uncalibrated cold reference (Deep Space) spectra averaged over N^{ma} measurements, expressed in [d.u.] at channel center "n", and corrected for nonlinearity. Uncalibrated instrument counts for nth channel on sensor wavenumber grid for FOV "p", sweep direction "d" and band "b"

$\left\langle \tilde{S}^{it}_{b,p,d}\left[n\right] \right\rangle$ complex uncalibrated hot reference (ICT) spectra averaged over N^{ma} measurements, expressed in [d.u.] at channel center "n", and corrected for nonlinearity. Uncalibrated instrument counts for nth channel on sensor wavenumber grid for FOV "p", sweep direction "d" and band "b"

λ_L Average metrology laser wavelength computed from current engineering packet neon calibration data (See Section 7.4.1)

Calibration Data

See parameters in Section 7.5.2 for ICT radiance calculation

ILS Parameters

Ancillary Data

Determined from instrument characterization. See description of ICT radiance parameters and calculation in Section 7.5.2.

N_b Number of output spectral bins

Work Data

See Section 7.5.2 for mean calculation of ICT telemetry components (SSM baffle temp, ICT PRT1 temp, ICT PRT2 temp, OMA1 temp, OMA temp).

Local Variables

$\sigma_b[0]$ wavenumber of channel having n = 0 [cm^{-1}] (sensor wavenumber grid)

$\Delta\sigma_b$ channel spacing [cm^{-1}]; sensor wavenumber grid

$\sigma_b[n]$ wavenumber of nth channel center [cm^{-1}] (sensor wavenumber grid)

$\sigma_b'[0]$ wavenumber of channel having n = 0 [cm^{-1}] (user wavenumber grid)

$\Delta'\sigma_b$ channel spacing [cm^{-1}]; user wavenumber grid

$\sigma_b'[n]$ wavenumber of nth channel center [cm^{-1}] (user wavenumber grid)

λ_S metrology sampling interval (cm) ($\lambda_s = \lambda_L/2 \approx 775x10^{-7} cm$). The sampling interval is half the laser metrology wavelength

$L_b^{ict}[n']$ is the calculated radiance for the hot calibration reference (the ICT), calculated on the user wavenumber scale

$E_{b,p,i}^{pol}[n']$ is the polarization induced calibration bias at scene select mirror angle δ^s (see section 3.2)

Operators

$F_b\left[n,n'\right]$ is the spectral resampling matrix operator (see section 3.5). Correction of the Doppler shift due to the relative velocity between the observation location and the spacecraft associated with the Earth's rotation is completed within the resampling operator.

$f_{ATBD_b}\left[n\right]$ is the band guard filter (see section 3.6.5);

SA_s^{-1} is the self-apodization removal matrix operator (see section 3.6.2);

p Field of view (FOV);

b band

d sweep direction

predictICTrad_L1b{} is the function that computes the ICT predicted radiance from model inputs (see Section 5.4 and 7.5.2 for more details).

Output Variables

$\tilde{L}_{b,p,d}^{es}\left[n'\right]$ is the calibrated scene radiance on the user wavenumber scale;

flags Quality flags as defined in NASA Cross Track Infrared Sounder (CrIS) Level 1B Quality Flags Description Document

7.5.1 Radiometric Complex Calibration

Radiometric calibration transforms the digital count signal into radiance units. The complex calibration method is used for the radiometric calibration process. This method also corrects for the instrument phase. Polarization correction is included in the NASA L1B processing.

Refer to Section 7.5 for the complete CrIS specific calibration equation.

7.5.1.1 Definition of Variables

Refer to Section 7.5 for the definition of variables.

7.5.1.2 Exception Handling

The sweep direction "*d*" of the ICT and DS spectra must be selected to match the sweep direction "*d*" of the Earth scene when performing radiometric complex calibration.

7.5.2 ICT Radiance Calculation

Section 7.5.2 is theoretically consistent with the CrIS SDR ATBD. However, in the NASA L1B software, the Planck radiance is computed on the on-axis user grid.

7.5.3 Spectrum Correction

Spectrum correction includes application of the band-guard filter, the self-apodization removal matrix operator, and the spectral resampling matrix operator. A spectral correction that accounts for the Doppler effect resulting from relative motion between the spacecraft and the observed Earth scene is also applied in the Spectrum Correction module. In the Version 3 release, this correction currently only includes correction of the relative motion due to Earth rotation, which is the largest source of Doppler shift. The Doppler shift correction is performed within the resampling operator. The band-guard filter is applied before and after the self-apodization removal matrix operator. All operations are applied to both the numerator and denominator of the calibration equation.

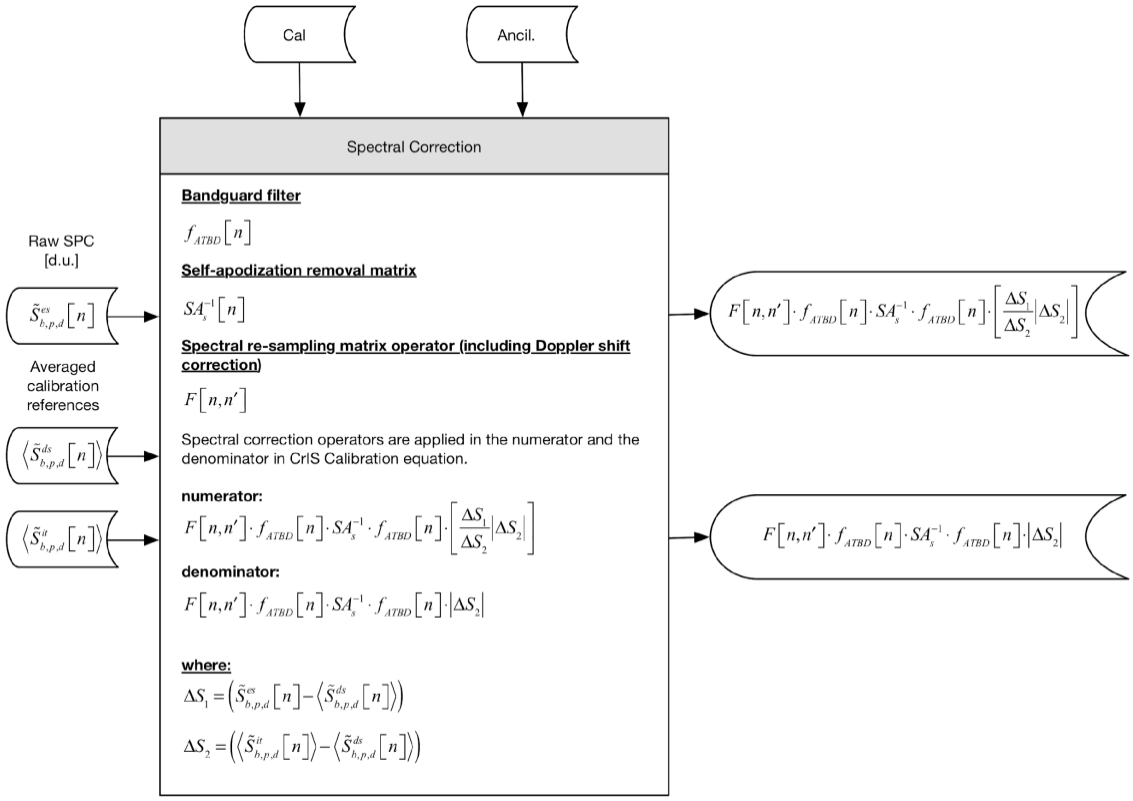

Figure 7.5.3- 1. Spectral Correction.

Refer to Section 7.5 for the complete CrIS L1B radiometric calibration equation.

7.5.3.1 Definition of Variables

Input variables

$\tilde{S}^{es}_{b,p,d}[n]$ is the complex uncalibrated Earth scene spectrum, expressed in [d.u.] at channel center "n", prior to nonlinearity correction. Uncalibrated instrument counts for nth channel on sensor wavenumber grid for FOV "p", sweep direction "d" and band "b"

$\left\langle \tilde{S}^{ds}_{b,p,d}[n] \right\rangle$ complex uncalibrated cold reference (Deep Space) spectra averaged over N^{ma} measurements, expressed in [d.u.] at channel center "n", and corrected for nonlinearity. Uncalibrated instrument counts for nth channel on sensor wavenumber grid for FOV "p", sweep direction "d" and band "b"

$\left\langle \tilde{S}^{it}_{b,p,d}[n] \right\rangle$ complex uncalibrated hot reference (ICT) spectra averaged over N^{ma} measurements, expressed in [d.u.] at channel center "n", and corrected for nonlinearity. Uncalibrated instrument counts for nth channel on sensor wavenumber grid for FOV "p", sweep direction "d" and band "b"

Calibration data

ILS parameters

Self-apodization removal matrix (calculated offline for sensor dependent nominal metrology laser wavelength $\lambda^{b}_{L,ISA}$, see section 3.6.3)

λ^{b}_{L} Average metrology laser wavelength computed from current engineering packet neon calibration data (See Section 7.4.1)

Ancillary data

N_b Number of output spectral bins

$\lambda^{b}_{S}(opt)$ Spectral sampling interval in band "b" for the user wavenumber scale (used in $F[n,n']$ matrix)

λ^{b}_{S} Spectral sampling interval in band "b" for the on-axis sensor wavenumber scale (used in $F[n,n']$ matrix)

Local variables

n Row index for matrix

n' Column index for matrix

$f_{ATBD}[n]$ Bandguard filter defined for each band (see section 3.6.5)

$F[n,n']$ Spectral resampling/interpolator matrix operator (see section 3.5) including Doppler shift correction (see section 3.9)

$SA_{b,p}^{-1}[n,n']$ Inverse self-apodization matrix operator (see Section 3.6.3)

7.5.3.2 CMO Computation

The spectral operators (bandguard filter, spectral resampling, Doppler correction, self-apodization removal, and Hamming apodization) are not combined into a single CMO matrix and Hamming apodization is not applied within the NASA L1B calibration.

7.5.3.3 Exception Handling

The inverse self apodization matrix is calculated offline for each band "b" using a sensor dependent nominal laser metrology sampling wavelength value, $\lambda_{L,ISA}^{b}$. The current laser metrology sampling wavelength for band "b" (λ_{L}^{b}) is determined from the spectral calibration module (based on the neon count). If λ_{L}^{b} differs from $\lambda_{L,ISA}^{b}$ by more than a predefined threshold, the ISA degraded QF is set to 1.

7.5.4 Non-linearity Correction

Section 7.5.4 is theoretically consistent with the CrIS SDR ATBD.

7.5.5 Polarization Correction

When considering the calibration bias due to polarization, representing the scene select mirror and sensor as a series pair of partial linear polarizers helps provide insight into the problem. The first polarizer represents the polarization due to the scene select mirror and the second polarizer represents the sensor polarization sensitivity. While the level of polarization is constant for the scene select mirror and sensor individually, the combined polarization due to the scene select mirror and the sensor is a function of the relative angle between the scene select mirror polarization axis which changes with rotation of the scene select mirror, and the instrument polarization axis, which is at a fixed angle. Thus, the combined polarization depends on the scene mirror rotation angle, and the rotation of the reflection plane at the scene mirror will create a modulation of the measured signal (see Section 3.2).

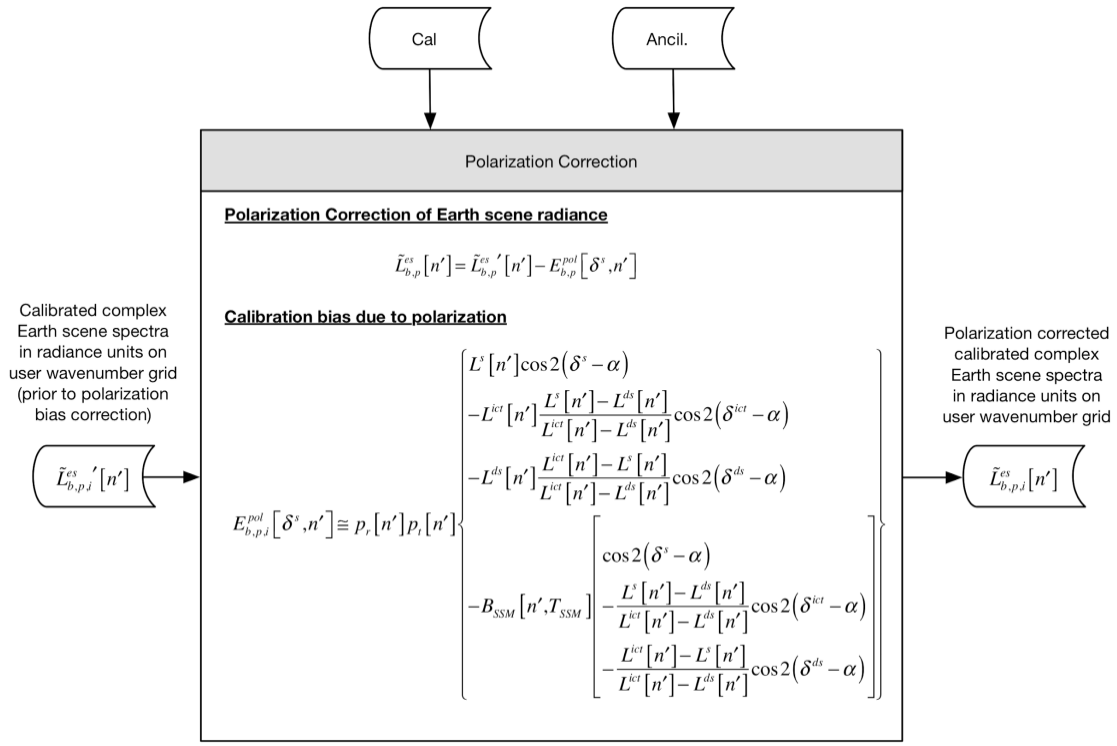

Figure 7.5.5- 1. Correction of calibration bias due to polarization.

7.5.5.1 Definition of Variables

Input variables

$L^{es}_{b,p,i}{}'[n']$ is the calibrated Earth scene radiance for nth channel on the user wavenumber grid for FOV “p”, FOR “i” and band “b”, prior to polarization correction

Calibration data

T_{SSM} Scene select mirror temperature (used to calculate the Planck radiance $B_{SSM}[n', T_{SSM}]$)

$\delta^s_{b,p,i}$ Scene mirror angle for FOV “p”, band “b”, and FOR “i”

$\alpha_{b,p}$ instrument polarization axis angle for band “b” and FOV “p”

$p_{r_{b,p}}[n']$ polarization of the scene select mirror (for band “b”, FOV “p”)

$p_{t_{b,p}}[n']$ polarization of the sensor (for band “b”, FOV “p”)

Ancillary data

N_b Number of output spectral bins (for band “b”)

Local variables

$E_{b,p,i}^{pol}\left[n'\right]$ is the polarization induced calibration bias at scene select mirror angle δ^s (see section 3.2)

Operators

p Field of view (FOV)

b band

i Field of regard

Output variables

$L_{b,p,i}^{es}\left[n'\right]$ is the calibrated Earth scene radiance corrected for calibration bias due to polarization for the n^{th} channel on the user wavenumber grid for FOV “p”, FOR “i” and band “b”

7.5.5.2 Exception Handling

Not applicable.

7.6 Quality Control

No change.

7.6.1 NEdN Estimation

The NEdN estimate is based on the standard deviation of the calibrated ICT radiances for the granule. The calibrated ICT measurements provide ability to calculate an NEdN estimate based on the stable ICT target temperature. The full radiometric and spectral complex calibration is applied to the ICT views for the NEdN estimate and uses the exact same algorithm that is applied to the calibration of the Earth scene measurements. Polarization correction and Doppler correction are not required or applied for completing the NEdN estimate.

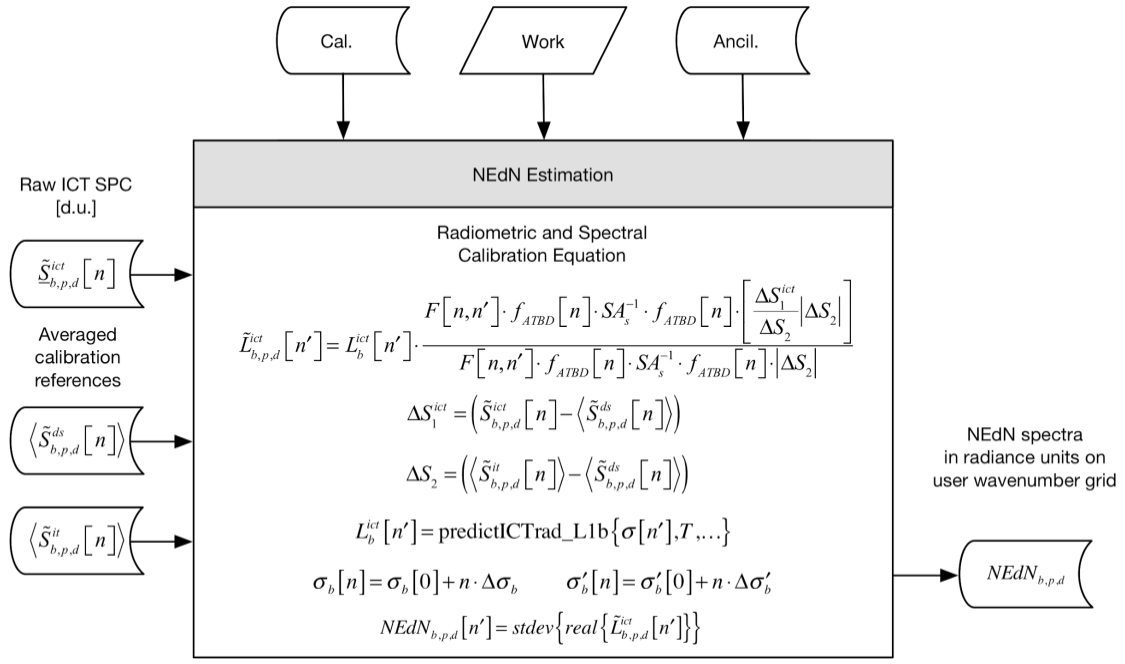

Figure 7.6.1- 1. NEdN estimation flowchart.

7.6.1.1 Definition of Variables

Input Variables

$\tilde{S}^{ict}_{b,p,d}[n]$ complex uncalibrated ICT spectra, expressed in [d.u.] at channel center “n”, and uncorrected for nonlinearity

$\left\langle \tilde{S}^{ds}_{b,p,d}[n] \right\rangle$ complex uncalibrated cold reference (Deep Space) spectra averaged over N^{ma} measurements, expressed in [d.u.] at channel center “n”, and corrected for nonlinearity;

$\left\langle \tilde{S}^{it}_{b,p,d}[n] \right\rangle$ complex uncalibrated hot reference (ICT) spectra averaged over N^{ma} measurements, expressed in [d.u.] at channel center “n”, and corrected for nonlinearity;

Calibration data from engineering packet

See parameters in Section 7.5.2 for ICT radiance calculation

Work variables

See Section 7.5.2 for mean calculation of ICT telemetry components (SSM baffle temp, ICT PRT1 temp, ICT PRT2 temp, OMA1 temp, OMA temp).

Local variables

$\sigma_b[0]$ wavenumber of channel having n = 0 [cm^{-1}] (sensor wavenumber grid)

$\Delta\sigma_b$ channel spacing [cm^{-1}]; sensor wavenumber grid

$\sigma_b[n]$ wavenumber of nth channel center [cm^{-1}] (sensor wavenumber grid)

$\sigma_b'[0]$ wavenumber of channel having n = 0 [cm^{-1}] (user wavenumber grid)

$\Delta'\sigma_b$ channel spacing [cm^{-1}]; user wavenumber grid

$\sigma_b'[n]$ wavenumber of nth channel center [cm^{-1}] (user wavenumber grid)

λ_S metrology sampling interval (cm) ($\lambda_s = \lambda_L/2 \approx 775x10^{-7} cm$). The sampling interval is half the laser metrology wavelength

$L_b^{ict}[n']$ is the calculated radiance for the hot calibration reference (the ICT), calculated on the user wavenumber scale

$\tilde{L}_{b,p,d}^{ict}[n']$ complex calibrated ICT radiance on the user wavenumber scale

Operators

$F_b[n,n']$ is the spectral resampling matrix operator (see section 3.5). Doppler correction is not included within the resampling operation during the NEdN calculation.

$f_{ATBD_b}[n]$ is the band guard filter (see section 3.6.5)

SA_s^{-1} is the self-apodization removal matrix operator (see section 3.6.2)

p Field of view (FOV)

b band

d sweep direction

predictICTrad_L1b{} is the function that computes the ICT predicted radiance from model inputs (see Section 5.4 and 7.5.2 for more details).

Output variables

$NEdN_{b,p,d}[n']$ NEdN estimate for nth channel on user wavenumber output grid

7.6.2 Fringe Count Error Handling

Not implemented in this version.

7.6.3 Fringe Count Error Detection

Not implemented in this version.

7.6.4 Fringe Count Error Correction

Not implemented in this version.

7.6.5 Data Quality Indicators

The NASA L1B software produces Quality Flag (QF) variables describing the quality of the primary data products. The individual flags in the QF variables are specific to the CrIS L1B algorithm and therefore are different from the flags in the SDR product.

For guidance on using QFs, refer to the “NASA Cross Track Infrared Sounder (CrIS) Level 1B Product Users’ Guide, Version 3, Rev A”.

For detailed information regarding the derivation and meaning of the individual flags that make up the CrIS L1B QF variable, refer to the “NASA Cross-track Infrared Sounder (CrIS) Level 1B Quality Flags Description Document, Version 3”. This document includes a mapping of the individual CrIS SDR quality flags to CrIS L1B quality flags where applicable.

7.7 Post-Processing

N/A.

7.7.1 User Required Spectral Bins Selection

N/A.

7.7.2 SDR Data Formatting

N/A.

7.8 Output Data Handling

The format of the CrIS L1B product is described in the NASA Cross Track Infrared Sounder (CrIS) Level 1B Product Users’ Guide, Version 3, Rev A.

8 CONCLUSION

The CrIS SDR ATBD defines the Level 1B algorithms needed on the ground in order to produce meaningful data meeting all the requirements of the CrIS instrument. This document identifies only the changes to the CrIS SDR ATBD document necessary to describe the algorithm used to produce the Version 3 NASA CrIS L1B radiance data product.

9 APPENDICES

9.1 Fast Fourier Transforms

No change.

9.1.1 Comments on Various Algorithms

No change.

9.1.2 Data Translation and Centering

No change.

9.1.3 Prime Factor Algorithm Fast Fourier Transform

No change.

9.2 Alias Unfolding

No change.

9.3 Linear Fitting

No change.

9.3.1 Implementation of the Linear Interpolation

No change.

9.4 Numerical Integration

No change.

9.5 Determination of the Goodness of Fit

No change.

9.6 Definitions

No change.

9.6.1 Sensor Calibration

No change.

9.6.2 Raw Data Record (RDR)

No change.

9.6.3 Sensor Data Record (SDR)

No change.

9.6.4 Environmental Data Record (EDR)

No change.

9.6.5 Data Product Levels

No change.

9.6.6 Measured Data

No change.

9.6.7 Auxiliary Data

No change.

9.6.8 Ancillary Data

The CrIS L1B algorithm requires Leap Seconds and UTC Polar Wander files. These requirements are described in the “CrIS L1B Software Users’ Guide, Version 3.0”.

9.6.9 Other Instrument Specific Terms and Definitions

No change.

— End of document —